

# 1 **MICS1 is the Ca<sup>2+</sup>/H<sup>+</sup> antiporter of mammalian mitochondria**

2

3 Shane Austin<sup>1\*#</sup>, Ronald Mekis<sup>1,2\*</sup>, Sami E. M. Mohammed<sup>2\*</sup>, Mariafrancesca Scalise<sup>3</sup>,  
4 Christina Pfeiffer<sup>1</sup>, Michele Galluccio<sup>3</sup>, Tamara Borovec<sup>1,2</sup>, Katja Parapatics<sup>4</sup>, Dijana Vitko<sup>4</sup>,  
5 Nora Dinhopf<sup>5</sup>, Keiryn L. Bennett<sup>4</sup>, Cesare Indiveri<sup>3</sup>, Karin Nowikovsky<sup>1,2§</sup>

6 1. Department of Internal Medicine I and Comprehensive Cancer Center, Medical University  
7 of Vienna, Austria

8 2. Department of Medical Sciences Institute for Biophysics and Physiopathology, University  
9 of Veterinary Medicine, Vienna, Austria

10 3. Department DiBEST (Biologia, Ecologia, Scienze della Terra) Unit of Biochemistry and  
11 Molecular Biotechnology, University of Calabria, Arcavacata di Rende, Italy

12 4. CeMM Research Center for Molecular Medicine of the Austrian Academy of Sciences,  
13 Vienna, Austria

14 5. Department of Pathobiology, Institute of Pathology, University of Veterinary Medicine,  
15 Vienna, Austria

16 # Present affiliation and address: Department of Biological & Chemical Sciences, The  
17 University of the West Indies, Cave Hill Campus, Barbados

18 \* Equal contribution

19 § Corresponding author: [karin.nowikovsky@vetmeduni.ac.at](mailto:karin.nowikovsky@vetmeduni.ac.at)

20 Keywords: mitochondria; Ca<sup>2+</sup>/H<sup>+</sup> Exchanger; mitochondrial metabolism; MICS1/TMBIM5;  
21 LETM1; Permeability Transition Pore

## 22 **Abstract**

23 Mitochondrial  $\text{Ca}^{2+}$  ions are crucial regulators of bioenergetics, cell death pathways and  
24 cytosolic  $\text{Ca}^{2+}$  homeostasis. Mitochondrial  $\text{Ca}^{2+}$  content strictly depends on  $\text{Ca}^{2+}$  transporters.  
25 In recent decades, the major players responsible for mitochondrial  $\text{Ca}^{2+}$  uptake and release  
26 have been identified, except the mitochondrial  $\text{Ca}^{2+}/\text{H}^+$  exchanger (CHE). Originally identified  
27 as the mitochondrial  $\text{K}^+/\text{H}^+$  exchanger, LETM1 was also considered as a candidate for the  
28 mitochondrial CHE. Defining the mitochondrial interactome of LETM1, we identified MICS1,  
29 the only mitochondrial member of the TMBIM family. Applying cell-based and cell-free  
30 biochemical assays, here we demonstrate that MICS1 is responsible for the  $\text{Na}^+$ - and  
31 permeability transition pore- independent mitochondrial  $\text{Ca}^{2+}$  release and identify MICS1 as  
32 the long-sought mitochondrial CHE. This finding provides the final piece of the puzzle of  
33 mitochondrial  $\text{Ca}^{2+}$  transporters and opens the door to exploring its importance in health and  
34 disease, and to developing drugs modulating  $\text{Ca}^{2+}$  exchange.

35

## 36 **Introduction**

37 Ion homeostasis is important for maintaining mitochondrial function. The dynamic balance of  
38 ions to maintain function is achieved by various cycles, which facilitate the interplay of  
39 cations, via the  $\text{K}^+$ ,  $\text{Na}^+$ , and  $\text{Ca}^{2+}$  cycles. Loss of this balance leads to several consequences in  
40 the organelle and ultimately the cell. These include mitochondrial swelling, disrupted cristae  
41 structure, deregulated bioenergetics and may result in cell death. Intracellularly,  
42 mitochondria have been established as major sinks of  $\text{Ca}^{2+}$ , an ion of comparatively low  
43 concentration to  $\text{K}^+$  and  $\text{Na}^+$ . The role of mitochondrial  $\text{Ca}^{2+}$  buffering has been extensively

44 studied (Giorgi et al., 2018; Pallafacchina et al., 2018), yet some of the players in maintaining  
45 this  $\text{Ca}^{2+}$  balance have not been identified (De Stefani et al., 2016; Urbani et al., 2020). One of  
46 the missing pieces in this molecular puzzle is the  $\text{Na}^+$ -independent  $\text{Ca}^{2+}$  efflux pathway, a  
47 putative  $\text{Ca}^{2+}/\text{H}^+$  exchanger (CHE). This exchanger, whose existence has been postulated since  
48 the 1970s (Carafoli et al., 1974) is critical for maintaining mitochondrial  $\text{Ca}^{2+}$  levels and plays  
49 an important role in mitochondrial functions.

50 To date, several studies have investigated the molecular identity of mitochondrial CHE, one  
51 of the likely candidates being LETM1. LETM1 first attracted interest when it was found to be  
52 associated with seizures in the Wolf Hirschhorn syndrome (Endele et al., 1999). Over the  
53 years, numerous studies characterized LETM1, a single transmembrane domain-containing  
54 protein, as the mitochondrial  $\text{K}^+/\text{H}^+$  exchanger (KHE) (Hasegawa and van der Blik, 2007;  
55 Hashimi et al., 2013; McQuibban et al., 2010; Nowikovsky et al., 2004; Nowikovsky et al.,  
56 2007). The proposal that LETM1 could be the CHE was based on a *Drosophila* S2 genome-wide  
57 RNAi screen of modulators of mitochondrial  $\text{Ca}^{2+}$  transport (Jiang et al., 2009). Subsequent  
58 studies have confirmed an involvement of LETM1 in  $\text{Ca}^{2+}$  and  $\text{K}^+$  transport but key questions  
59 remained (Austin and Nowikovsky, 2019, 2021; Nowikovsky and Bernardi, 2014). Perhaps the  
60 most important is how can a single transmembrane protein mediate a process of ion  
61 exchange, and it appeared possible that LETM1 could fulfill its function(s) as a multimer, or as  
62 part of a protein complex. The first possibility was addressed by Shao et al., who presented  
63 cryo EM structures of LETM1 oligomers, which facilitated pH-dependent movement of  $\text{Ca}^{2+}$  in  
64 a cell-free system (Shao et al., 2016). Whether LETM1 is part of a protein complex remains  
65 unaddressed.

66 In this study, we searched for partners of LETM1 and found the interactor mitochondrial  
67 Morphology and Cristae Structure 1 (MICS1), a member of the TMBIM family, which has been  
68 implicated in the regulation of intracellular  $\text{Ca}^{2+}$  by a number of studies (Carrara et al., 2012;  
69 Hung et al., 2011; Kim et al., 2021; Lisak et al., 2015; Liu, 2017; Rojas-Rivera and Hetz, 2015).  
70 Interestingly, MICS1 is the only species with a mitochondrial localization (Oka et al., 2008)  
71 while other TMBIM family members are localized to the ER, Golgi and the plasma membrane  
72 (Rojas-Rivera and Hetz, 2015). Functional characterization of the TMBIM family members has  
73 been generally addressed with mammalian cell culture and animal models, especially  
74 investigating their role in  $\text{Ca}^{2+}$  regulation. In fact, MICS1 was identified as a regulator of  
75 calcium and apoptosis (Lisak et al., 2015; Oka et al., 2008). Here, we demonstrate that MICS1  
76 is the long-sought mitochondrial CHE, a crucial component of mitochondrial  $\text{Ca}^{2+}$   
77 homeostasis.

78

## 79 **Results**

### 80 **MICS1 interacts with LETM1**

81 We determined the interactome of LETM1 using affinity purification mass spectrometry (AP-  
82 MS) from whole cell lysates and isolated mitochondria (**Figure 1A**). As few studies have used  
83 the limited amounts of material from isolated organelles for AP-MS, we assessed the  
84 suitability of our modified method to investigate organellar interactomes (**Figure 1–figure**  
85 **supplement 1A**). Using the mitochondrial  $\text{Ca}^{2+}$  uniporter (MCU) as a benchmark inner  
86 mitochondrial membrane protein, we confirmed the ability of our method to detect the  
87 members of the published core interactome except for the tertiary interactor MICU2, which  
88 interacts with MICU1 (Sancak et al., 2013) (**Figure 1–figure supplement 1B**). Thus, the method

89 was sufficiently robust to cover approximately 75% of a mitochondrial core interactome  
90 (**Figure 1– figure supplement 1C**). We then determined the LETM1 interactome. Data  
91 obtained from both the whole cell and isolated mitochondria data sets were reproducible  
92 with an overlap of 31 proteins that interacted in both approaches (**Figure 1– figure**  
93 **supplement 1D**) including TBK1, a protein previously observed to interact with LETM1 in  
94 similar AP-MS studies (Li et al., 2011).

95 One protein that was immediately of interest was MICS1, which is an inner mitochondrial  
96 membrane protein with 6-8 transmembrane domains depending on the prediction tool used.  
97 Similar to LETM1, MICS1 has already been shown to be involved in the regulation of  
98 mitochondrial structure (Oka et al., 2008; Seitaj et al., 2020).

99 Specifically relying on crudely isolated mitochondria to perform co-immunoprecipitation  
100 experiments, we were able to confirm that LETM1 does indeed interact with MICS1 (**Figure**  
101 **1B**). Probing for mitochondrial Prohibitin demonstrated this was not an enrichment of  
102 membrane-associated proteins, but rather a specific complex (**Figure 1B-left**). The same  
103 result was obtained when MICS1 was immune-precipitated, with LETM1 being present in the  
104 same complex (**Figure 1B-right**). LETM1 forms high molecular weight complexes migrating at  
105 approximately 400 and 720 kDa. Blue native gel electrophoresis (BNGE) detected LETM1  
106 and MICS1 in same complexes of 720 kDa and ~ 400 kDa (**Figure 1 C**). Applying low serum  
107 conditions to enhance MICS1 levels (Oka et al., 2008), the alterations of MICS1 amounts were  
108 paralleled by LETM1, while in contrast the amounts of the mitochondrial protein UQCRC2 did  
109 not change (**Figure 1D**).

110 **MICS1 depletion impairs mitochondrial bioenergetics and morphology**

111 Functional characterization of MICS1 being limited, we first generated MICS1 stable  
112 knockdown by short hairpins targeting various exons. Stable knockdown cells had up to 80 %  
113 reduced MICS1 levels compared to scrambled controls and were accompanied by a  
114 proportional decrease of LETM1 (**Figure 2A**). The proliferation rate of MICS1KD1 in glucose-  
115 containing media was modestly reduced compared to controls, with only the final time point  
116 being significantly affected (**Figure 2B**). While no significant difference in any respiratory  
117 parameter was observed with glucose as the substrate (**Figure 2C-D**), galactose-dependent  
118 respiration was severely compromised in MICS1KD cells (**Figure 2E-F**), indicating that MICS1  
119 impacts on mitochondrial function. To further address the specific function of MICS1 in  
120 mitochondrial morphology and cation homeostasis, we generated MICS1 knockout HEK293  
121 and HeLa cells by CRISPR/Cas9 genome editing. At the gene expression level, we obtained  
122 HEK293 and HeLa knockout individual clones that entirely abrogated the transcript levels of  
123 MICS1. At the protein level, the total knockout was confirmed in HeLa cells clone IIF3 (HeLa  
124 MICS1KO) and in HEK293 cells clone IIF1 (HEK293 MICS1KO#1). In several other clones,  
125 translation was not entirely abolished, like in HEK293 clone IE12 (HEK293 MICS1KO#2) (**Figure**  
126 **3A and E**). Comparison of HEK293 cell proliferation rates indicated that while the complete  
127 loss of MICS1 did not affect cell growth, growth of mutant cells with residual MICS1  
128 expression was significantly slowed (**Figure 3B**), similarly to MICS1KD (**Figure 2B**), suggesting  
129 a potential cellular adaptation in a full KO.

130 We performed transmission electron microscopy to study mitochondrial ultrastructure of  
131 MICS1-deficient cells that had a null mutation or still had residual levels of the MICS1 protein.  
132 As previously shown for HeLa and HAP cells (Oka et al., 2008; Seitaj et al., 2020), compared  
133 to wild-type cells HEK293 MICS1KO#1 and MICS1KO#2 displayed fragmented and less  
134 elongated mitochondria, respectively (**Figure 3C**). Electron micrographs showed

135 mitochondria with swollen sections and altered cristae structures when MICS1 was deleted,  
136 cristae being also affected in the incomplete MICS1KO (**Figure 3D, arrows**). Since OPA1 is  
137 known to control cristae volume and cristae junction organization, which is a crucial  
138 determinant for mitochondrial cytochrome c retention (Del Dotto et al., 2017; Olichon et al.,  
139 2003), we investigated whether cristae changes were associated with changes in the cleavage  
140 pattern of OPA1 isoforms. Increased c and e subunits were apparent in both complete and  
141 partial KO compared to controls (**Figure 3E-F**). OPA1 c and e forms are the cleavage products  
142 of OMA1. We found significantly reduced levels of OMA1, in line with the autocatalytic  
143 degradation of activated OMA1 (**Figure 3E-F**). In addition, DRP1 was upregulated (**Figure 3E-**  
144 **F**), supporting the shift of the mitochondrial morphology towards increased fission and  
145 consistent with stress-sensitive activation of OMA1 and OMA1-dependent OPA1 cleavage.  
146 Our western blot analysis further confirmed the depletion of MICS1 in MICS1KO#1 and strong  
147 reduction in MICS1KO#2 and the proportional decrease of LETM1 (**Figure 3 E-F**).

#### 148 **Mitochondrial KHE requires LETM1 and MICS1**

149 Based on the interaction of MICS1 with LETM1 and on the implication of LETM1 in  
150 mitochondrial  $K^+/H^+$  exchange (Nowikovsky et al., 2012), we asked whether MICS1  
151 contributes to KHE activity. Light scattering methods have been classically used to monitor  
152 the swelling of mitochondria (Bernardi, 1999; Mitchell, 1966). Using acetate-based cationic  
153 salts to measure the swelling of isolated mitochondria is a robust and accurate method to  
154 assess relative KHE activity in these organelles. HeLa and HEK293 MICS1KO mitochondria had  
155 a significantly reduced rate of swelling in potassium acetate buffer (**Figure 4 A-D**), indicating  
156 reduced KHE activity, as also seen for both  $K^+$  and  $Na^+$  salts in mitochondria from LETM1KD  
157 cells (**Figure 4E-F**), see also (Austin et al., 2017). Re-expression of MICS1 in HeLa MICS1KO

158 cells restored swelling to wild-type levels (**Figure 4A-B**), confirming a correlation between  
159 MICS1 and KHE activity. Together with the proportional decrease of LETM1 in MICS1  
160 knockdown or knockout (**Figure 2A**), these data suggested that MICS1 depletion may reduce  
161 the KHE activity by destabilizing LETM1. Importantly, these findings demonstrate that LETM1-  
162 mediated active KHE activity requires the presence of MICS1.

### 163 **MICS1 mediates mitochondrial Na<sup>+</sup>-independent Ca<sup>2+</sup> efflux**

164 As the TMBIM protein family controls intracellular Ca<sup>2+</sup> and previous work has proposed a  
165 Ca<sup>2+</sup> channel function linked to pH sensitivity for the bacterial TMBIM homolog BsYetJ (Guo  
166 et al., 2019), we asked whether MICS1 controls mitochondrial Ca<sup>2+</sup> homeostasis by mediating  
167 Ca<sup>2+</sup>/H<sup>+</sup> exchange. To this end, we performed mitochondrial Ca<sup>2+</sup> uptake and release assays  
168 in digitonin-permeabilized HEK293 cells pulsed with external Ca<sup>2+</sup>. To focus on H<sup>+</sup>-dependent  
169 Ca<sup>2+</sup> fluxes and exclude Na<sup>+</sup>-dependent Ca<sup>2+</sup> fluxes, we used the NCLX inhibitor CGP37157.  
170 MICS1WT and MICS1KO mitochondria exhibited similar rates of energy-dependent Ca<sup>2+</sup>  
171 uptake (**Figure 5A and C and Figure 5-figure supplement 1**). The MCU inhibitor ruthenium  
172 red (RR) induced Ca<sup>2+</sup> release from wild-type mitochondria, confirming that mitochondria can  
173 extrude matrix Ca<sup>2+</sup> through an NCLX independent pathway, which is widely assumed to be a  
174 CHE. Residual matrix Ca<sup>2+</sup> was then initiated by the pore-forming peptide alamethicin, or by  
175 FCCP, the protonophore that collapses the proton gradient. Wild-type mitochondria released  
176 Ca<sup>2+</sup> to corresponding levels of total Ca<sup>2+</sup> uptake (**Figure 5A**). Remarkably, MICS1KO  
177 mitochondria displayed decreased to absent RR-induced mitochondrial Ca<sup>2+</sup> release, which  
178 was proportional to the depletion of MICS1 mitochondria (**Figure 5A-D** red and orange  
179 traces). Released total mitochondrial Ca<sup>2+</sup> through alamethicin reached similarly high level in



180 MICS1KO as in MICS1WT, confirming comparable levels of matrix  $\text{Ca}^{2+}$  (**Figure 5A**). Re-  
181 expression of MICS1 in HEK293 MICS1 KO was able to restore  $\text{Ca}^{2+}$  efflux (**Figure 5A**).

182 Since MICS1 and LETM1 interact, and LETM1 was proposed as the mitochondrial CHE, we next  
183 sought to address once again  $\text{Ca}^{2+}$  fluxes in HEK293 LETM1 KD under the same conditions. The  
184 presence or absence of LETM1 (**Figure 4–figure supplement 1**) did not alter  $\text{Ca}^{2+}$  uptake  
185 (**Figure 5–figure supplement 1**) nor the  $\text{Na}^+$ -independent  $\text{Ca}^{2+}$  fluxes (**Figure 5E-F**). To assess  
186 whether the permeability transition pore (PTP) contributes to the recorded  $\text{Ca}^{2+}$  fluxes, we  
187 repeated  $\text{Ca}^{2+}$  uptake/efflux assays in presence of cyclosporin A (CsA), the PTP desensitizer  
188 (Basso et al., 2008). MICS1WT displayed comparable  $\text{Ca}^{2+}$  efflux as in the absence of CsA,  
189 confirming that  $\text{Na}^+$ -independent  $\text{Ca}^{2+}$  release was also independent of PTP flickering or  
190 opening (**Figure 5G-H**). Addition of CsA hardly altered the rate or magnitude of  $\text{Ca}^{2+}$  release.  
191 Since deletion of MICS1 or LETM1 reduces KHE activity, we asked whether increasing KHE  
192 activity would restore  $\text{Ca}^{2+}$  release in MICS1KO mitochondria. Therefore, we repeated the  
193 previous experiment in the presence of nigericin, a highly selective ionophore catalyzing KHE,  
194 which did not restore  $\text{Ca}^{2+}$  efflux (**Figure 5I-J**). Thus, our results indicated that  $\text{Na}^+$ -  
195 independent  $\text{Ca}^{2+}$  efflux requires MICS1 but not LETM1 or LETM1-mediated KHE activity.

#### 196 **Thapsigargin-mobilized $\text{Ca}^{2+}$ induces PTP opening in MICS1KO cells**

197 The similar vigorous  $\text{Ca}^{2+}$  uptake by MICS1KO and -WT mitochondria but unequal  $\text{Ca}^{2+}$  release,  
198 unless alamethicin was used, raised the intriguing question of the fate of intramitochondrial  
199  $\text{Ca}^{2+}$ . To exclude the ER as a  $\text{Ca}^{2+}$  sink and deplete ER stores, we repeated  $\text{Ca}^{2+}$  uptake/release  
200 experiments using measurement media containing the SERCA pump inhibitor thapsigargin.  
201 MICS1WT mitochondria behaved as in the absence of thapsigargin, with identical rapid  $\text{Ca}^{2+}$   
202 influx, RR-induced  $\text{Ca}^{2+}$  efflux and FCCP-induced release of total free matrix  $\text{Ca}^{2+}$  (**Figure 5K**).

203  $\text{Ca}^{2+}$  uptake was comparable in MICS1WT and MICS1KO#1, while significantly slowed in  
204 MICS1KO#2 (**Figure S2**). In contrast, MICS1KO#1 and MICS1KO#2 mitochondria, which were  
205 refractory to  $\text{Ca}^{2+}$  efflux in absence of thapsigargin, released RR-induced  $\text{Ca}^{2+}$  with rates 4-6  
206 times higher than in MICS1WT. The levels of  $\text{Ca}^{2+}$  efflux seemed saturated, as they almost  
207 reached those of total  $\text{Ca}^{2+}$  release after FCCP addition, which in presence of thapsigargin  
208 were comparable to those of MICS1WT (**Figure 5K-L**). These drastic effects of thapsigargin on  
209 mitochondrial RR-induced  $\text{Ca}^{2+}$  efflux observed when MICS1 was deleted and NCLX inhibited,  
210 suggested stimulation of the CHE or opening of the PTP, which could both be caused by  
211 increased matrix  $\text{Ca}^{2+}$  load. Consistent with PTP opening (Beghi and Giussani, 2018), RR-  
212 induced  $\text{Ca}^{2+}$  release was accompanied by significant depolarization of MICS1KO but not  
213 MICS1WT mitochondria as indicated by the membrane potential dye TMRM (**Figure 5M-N**).  
214 To verify the PTP  $\text{Ca}^{2+}$ -sensitivity and evaluate the total free  $\text{Ca}^{2+}$  load tolerated by MICS1KO  
215 mitochondria, we performed  $\text{Ca}^{2+}$  retention capacity (CRC) assays. MICS1WT mitochondria  
216 exposed to thapsigargin in presence of CGP37157 tolerated 5  $\text{Ca}^{2+}$  pulses, corresponding to  
217 25  $\mu\text{M}$   $\text{Ca}^{2+}$  before PTP opening (**Figure 5O**). In contrast, MICS1KO#1 only tolerated 3  $\text{Ca}^{2+}$   
218 pulses, corresponding to 15  $\mu\text{M}$   $\text{Ca}^{2+}$  (**Figure 5P**). PTP desensitization with CsA increased the  
219 retention capacity to a very similar extent in MICS1KO and MICS1WT mitochondria (**Figure**  
220 **5O-P**). In the absence of CsA, the increased sensitivity to  $\text{Ca}^{2+}$ -induced PTP opening of  
221 MICS1KO#1 required NCLX inhibition, as without addition of CGP37157 the retention capacity  
222 was the same for MICS1WT and MICS1KO#1 mitochondria with 20  $\mu\text{M}$   $\text{Ca}^{2+}$  (**Figure 5-figure**  
223 **supplement 2**). The activation of PTP observed in **Figure 5K** indicated that thapsigargin  
224 increased the  $\text{Ca}^{2+}$  load in MICS1KO mitochondria. Likely, by inducing higher  $\text{Ca}^{2+}$  uptake rates  
225 or mobilizing an additional source of matrix  $\text{Ca}^{2+}$ , and lowering the threshold for tolerated  
226  $\text{Ca}^{2+}$ , which would reduce  $\text{Ca}^{2+}$  buffering capacity. The CRC results confirmed the sensitization

227 to Ca<sup>2+</sup>-induced PTP opening when NCLX is inhibited (Luongo et al., 2017). Consistent with a  
228 role of PTP opening in the large Ca<sup>2+</sup> release observed in MICS1KO mitochondria, addition of  
229 CsA and ADP prevented excess Ca<sup>2+</sup> release from MICS1KO mitochondria (**Figure 5Q-R**).

### 230 **Purified reconstituted MICS1 transports Ca<sup>2+</sup>**

231 To assess the mechanism and selectivity of MICS1-dependent in cation transport we  
232 produced purified MICS1 for reconstitution studies. Codon optimized hMICS1 cDNA (**Figure**  
233 **6–figure supplement 1A**) was cloned in pH6EX3 (Galluccio et al., 2013) and the recombinant  
234 construct was used to transform *E. coli* Rosetta cells. During the exponential phase of growth  
235 (OD ~ 0.8-1), the temperature was set to 37 °C and 0.4 mM IPTG was added to induce  
236 synthesis of the protein. MICS1 was over-expressed in the insoluble fraction of the induced  
237 cell lysate after 2 hours of IPTG induction (**Figure 6–figure supplement 1B**). The protein was  
238 purified by Ni-chelating chromatography and reconstituted in proteoliposomes to assess in  
239 vitro Ca<sup>2+</sup> transport activity assays using Calcium Green-5N as described Materials and  
240 Methods and illustrated in **Figure 6A**. The incorporation of MICS1 in proteoliposomes was  
241 verified by western blot analysis (**Figure 6B**). As shown in **Figure 6C-E**, reconstituted MICS1  
242 mediated Ca<sup>2+</sup> fluxes in a pH-dependent manner, with a maximum at pH 7.0 (**Figure 6D**) and  
243 inhibition of fluxes at pH 8.0 (**Figure 6E**). To further investigate the involvement of H<sup>+</sup> in the  
244 transport cycle, we measured H<sup>+</sup> flux using the pH sensitive dye pyranine (**Figure 6F**).  
245 Remarkably, alkalinization of the internal compartment of proteoliposomes detected by the  
246 increase in pyranine fluorescence indicated a H<sup>+</sup> flux towards the external compartment  
247 induced by Ca<sup>2+</sup> addition, i.e., concomitant to the inwardly directed Ca<sup>2+</sup> flux (**Figure 6A**).

248

### 249 **Discussion**

250 The role and selectivity of LETM1 as an ion transporter/channel has not been unequivocally  
251 assessed. The open questions remained whether it transports  $K^+$  or  $Ca^{2+}$ , and whether it  
252 operates as an exchanger or rather as a component of the transport system. The work by  
253 Shao et al. showed that purified LETM1 oligomerizes into a high molecular weight complex of  
254  $> 404$  kDa, which forms a central cavity that undergoes pH-dependent conformational  
255 changes (Shao et al., 2016). In line with other reports, they proposed that LETM1 is a  
256 mitochondrial CHE (Doonan et al., 2014; Jiang et al., 2013). However, other studies clearly  
257 demonstrated that LETM1 plays a key role in mitochondrial  $K^+$  transport (Austin et al., 2017;  
258 Hashimi et al., 2013; Nowikovsky et al., 2012). The unresolved identity of the mitochondrial  
259 CHE and the controversy on LETM1 motivated us to further search for LETM1 interactors that  
260 could functionally cooperate with LETM1 in mitochondrial  $K^+$  and/or  $Ca^{2+}$  efflux.

261 To address the relatively low mitochondrial protein yield from mammalian cell cultures, we  
262 developed a miniaturized proteomic approach that was validated with the MCU interactome  
263 as a model. Among the most promising identified interactors of LETM1, we focused on MICS1.  
264 Our study demonstrates that a complex containing LETM1 and MICS1 is involved in  $K^+/H^+$   
265 exchange in vivo, since decreased levels of both LETM1KD and MICS1KO led to a decrease of  
266  $K^+$  transport. This effect is likely due either to reduced LETM1 levels, also in absence of MICS1,  
267 or to loss of protein interaction, a possibility that will be further explored in future analyses  
268 of MICS1 and LETM1 mutations affecting their physical interaction. Comparison of the roles  
269 of MICS1 and LETM1 in mitochondrial  $Ca^{2+}$  efflux clearly showed that LETM1, unlike MICS1, is  
270 not required for CHE activity. In contrast to LETM1, loss of MICS1 abrogated the function of  
271 CHE, which was restored by re-expression of MICS1. Independent of any interaction partner  
272 or protein complex, reconstituted MICS1 was able to transport  $Ca^{2+}$  across proteoliposomes

273 in a pH-dependent manner and to drive Ca<sup>2+</sup>-dependent H<sup>+</sup> transport. Thus, based on the  
274 consistency between cellular and cell-free activity of MICS1 in Na<sup>+</sup>-independent  
275 mitochondrial Ca<sup>2+</sup> translocation, we have identified MICS1 as the long-sought mitochondrial  
276 CHE. Interestingly, MICS1 does not belong to any mitochondrial carrier family. The MICS1  
277 structure predicted by AlphaFold (Jumper et al., 2021) shows a typical fold of membrane  
278 proteins with transport function with eight transmembrane segments and a long unresolved  
279 extra membrane domain (**Figure 6–figure supplement 1C**). MICS1 has no homologue in yeast  
280 *S. cerevisiae*, which lacks a mitochondrial Ca<sup>2+</sup> uptake pathway.

281 As previously shown (Oka et al., 2008) and clearly confirmed here, loss of MICS1 causes  
282 changes in mitochondrial morphology. Our data additionally demonstrate that the  
283 morphological alterations are matched by reduced respiratory capacity that becomes evident  
284 with galactose as a substrate. The basis of this may reside in perturbation of Ca<sup>2+</sup> homeostasis  
285 leading to excessive Ca<sup>2+</sup> accumulation and possibly alterations of K<sup>+</sup> homeostasis linked to  
286 secondary effects on LETM1. Thus, our findings link mitochondrial dysfunction to cation  
287 deregulation and provide a solid molecular framework for future studies.

288 The lack of a functional CHE also has severe implications on the permeability transition when  
289 Na<sup>+</sup> dependent Ca<sup>2+</sup> efflux is concomitantly blocked, as revealed by thapsigargin-induced  
290 hypersensitization of PTP opening. One reason that may explain why MICS1KO mitochondria  
291 are so sensitive to the PTP opening is reduced levels of Sirt3, which is responsible for  
292 deacetylation of CypD, a key PTP sensitizer (Sambri et al., 2020). The result is in accordance  
293 with the modulatory effect of thapsigargin on shifting the ratio between bound and free Ca<sup>2+</sup>  
294 towards free Ca<sup>2+</sup> (Korge and Weiss, 1999). The hypersensitivity of Ca<sup>2+</sup>-induced PTP opening  
295 also correlates with the observed cristae reorganization, OPA1 cleavage pattern and OMA1

296 activation, which could explain increased predisposition to cell death in MICS1KO cells  
297 exposed to thapsigargin.

298 In conclusion, the use of cell free and cell culture models has allowed us to demonstrate that  
299 MICS1 is the mitochondrial CHE. In view of the established involvement of LETM1 in both KHE  
300 and CHE activity, the identification of the LETM1 partner MICS1 is also a major step forward  
301 in resolving current controversies on their relative role in mitochondrial  $\text{Ca}^{2+}$  and  $\text{K}^{+}$   
302 homeostasis. Indeed, we have demonstrated that MICS1 is a necessary part of the KHE  
303 machinery and its interaction with LETM1 fulfills a physiological role in the cell and in  
304 maintaining  $\text{Ca}^{2+}$  balance. Further investigation of LETM1 and MICS1 interaction partners will  
305 shed further light on the regulatory mechanism maintaining mitochondrial ion balance.

306

## 307 **Material and Methods**

### 308 **Reagents**

309 All reagents used in this study were from Sigma Aldrich, unless otherwise indicated.

310 Antibiotics: normocin, blasticidin, hygromycin, puromycin and doxycycline were from  
311 Invivogen (San Diego, CA). Restriction endonucleases and specific reagents for cloning, Pierce  
312 BCA protein assay kit, Glutaraldehyde, lead citrate, propylene oxide and osmium tetroxide  
313 were from Merck (Darmstadt, Germany), ProtA/G agarose and DMEM (#41966-029) from  
314 Thermo Fisher Scientific, NativeMark™ #LC0725) NativePAGE™ 3-12 % Bis-Tris Protein, #  
315 BN1001), Turbofect,  $\text{Ca}^{2+}$  Green 5N, and MitoTracker™ Green FM (#M7514) from Invitrogen,  
316 Streptactin beads from IBA-lifesciences. Bradford was from BioRad, Proteinase inhibitor from  
317 Roche (Basel, Switzerland), C12E8 from TCI Europe, TMRM from Molecular Probes, Glycid

318 ether 100 from Serva (Heidelberg, Germany). Fetal Bovine Serum (FBS), and pen/strep were  
319 from Gibco. Mycoplasma test kit was from MycoAlert Lonza kit. The working concentration  
320 of Ruthenium red was calculated with Lambert-Beer law,  $A=533 \text{ nm}$ ,  $l = 1 \text{ cm}$ ,  $\epsilon = 65000$ .

### 321 **Antibodies used in this study**

322 LETM1 (Abnova, #H00003954), 1:1000, LETM1 (Santa Cruz Biotechnology, #sc-163013),  
323 1:1000, LETM1 C-terminal region (Aviva, Systems Biology, #OAAB12878), 1:1000, MICS1  
324 (Abcam, #ab106754), 1:1000, MICS1 (Aviva systems biology, #OAAF06415), 1:1000, OPA1 (BD  
325 Biosciences, #612606), 1:1000, SIRT3 (Cell Signaling Technology, #5490), 1:1000, DRP1 (Santa  
326 Cruz Biotechnology, #sc-271583), 1:1000, HSP60 (Santa Cruz Biotechnology, #sc-1052),  
327 1:1000, TOM20 (Cell Signaling Technology, #42406), 1:1000, TOM40 (Santa Cruz  
328 Biotechnology, #sc-365467), 1:1000, OMA1 (Santa Cruz Biotechnology, #sc-515788), 1:1000,  
329 Prohibitin (Abcam, #ab210082), 1:1000,  $\beta$ -Actin (Invitrogen, #MA5-11869), 1:1000,  
330 PolyHistidine-Peroxidase (Sigma Aldrich, #a7058), 1:10000, Goat- $\alpha$ -mouse (Jackson  
331 ImmunoResearch, #115-035-003) 1:5000, Rabbit- $\alpha$ -goat (Jackson ImmunoResearch, #305-  
332 035-003) 1:5000, Goat- $\alpha$ -rabbit (Jackson ImmunoResearch, #111-035-144) 1:5000.

### 333 **Cell culture**

334 HEK293 Flp-In T-Rex (Invitrogen), HeLa (Austin et al., 2017) and HEK293 (ATCC) cells were  
335 maintained in DMEM supplemented with FBS (10% v/v), and penicillin/streptomycin  
336 (pen/strep) (1%). Cells were cultured in an incubator set to 37 °C and 5% CO<sub>2</sub> and splitted  
337 when reaching confluency of ~70-90%, and regularly tested for mycoplasma.

### 338 **Generation of knockdown and knockout cells**

339 All shRNA constructs for MICS1 and LETM1 were obtained from Origene Technologies  
340 (Rockville, MD). Primers were from Microsynth, Balgach, Switzerland. HeLa scramble and  
341 LETM1KD cells were described in (40). HEK293 scramble and LETM1 knockdown cells were  
342 generated using the short hairpin constructs from (Austin et al, 2017) in HEK293-Flp-In T-Rex  
343 cells. MICS1KD cells were generated using the human shRNA plasmid kit for MICS1 (Origene,  
344 TR315671B) with the shRNA construct #1 (GGTCTTGGAGCATTCTGCTACTATGGCTT) and  
345 construct #2 (GCCATAGCAATCAGCAGAACGCCTGTTCT and  
346 GGTCTCTTCTCATCAGAGCTGCATGGTA) used for stable KD cell lines. Cells were transfected  
347 with Turbofect according to the manufacturer instructions; 48 hrs post transfection the media  
348 was changed to selection media containing puromycin (2 µg/mL). Puromycin-resistant cell  
349 populations were maintained in growth media supplemented with puromycin (1 µg/mL).  
350 MICS1KO cells were generated by the Protein Technologies Facility at Vienna BioCenter Core  
351 Facilities (VBCF), member of the Vienna BioCenter (VBC), Austria. 4 gRNAs targeting GHITM  
352 were designed using CRISPOR tool (crispor.tefor.net). gRNAs were selected primarily on the  
353 criterium of their specificity (at least 3 mismatches with at least one in the seed region to any  
354 off-target) and on predicted activity according to Doench score. Guide 1:  
355 CCAAACAAGAATTGGGATC (targeting exon 3), guide 2: GCATTGTGCTACTATGGCTT (targeting  
356 exon 4), guide 3: CAGCCATTGATTCTTCGTGA (targeting exon 2) and guide 4:  
357 GGCTCCTCTGACAATATTA (targeting exon 7). Targeting sequences were introduced into  
358 pX459 Cas9-p2A-puro plasmid (Addgene 48139) via BbsI cloning. Plasmids (3 µg) were  
359 introduced into HEK 293 cells ( $1 \times 10^6$ ) by electroporation with Neon electroporator (Thermo  
360 Fisher Scientific) according to the manufacturers protocol. 24 hrs post electroporation cells  
361 were selected with puromycin (4 µg/ml) and 72 hrs later collected and lysed for genotyping.  
362 Editing efficiency was confirmed with TIDE algorithm (<https://tide.deskgen.com/>) based on



363 chromatogram analysis with WT HEK293 PCR product used as a reference. Guide 2  
364 (GCATTGTGCTACTATGGCTT) was selected for performing the KO in HEK and HeLa cells based  
365 on its highest activity (59.7%) and cloned into an in-house template vector p31 containing T7  
366 promoter followed by BbsI cloning sites, optimized gRNA scaffold and DraI restriction site  
367 used for template linearization. Resulting gRNA transcription was performed with HiScribe T7  
368 High Yield RNA Synthesis Kit (NEB) according to the manufacturer's protocol and gRNA was  
369 purified and verified for concentration and RNA integrity. 12 µg of gRNA pre-mixed with 5 µg  
370 Cas9 protein (2×NLS) in Cas9 buffer (20 mM HEPES pH 7.5, 150 mM KCl, 0.5 mM DTT, 0.1 mM  
371 EDTA) were used for electroporation of 70-80 % confluent cells. Electroporated cells were  
372 cultured in DMEM supplemented with 10 % FCS and L-Gln. Normocin was added after  
373 approximately 2 hrs, and after 24 hrs genotyping was performed to confirm editing.

#### 374 **Mitochondria isolation**

375 Frozen cell pellets were thawed and resuspended in isolation media (Austin et al., 2017)  
376 containing 1.7 mM Proteinase inhibitor cocktail. Cells were homogenized on ice with 12  
377 strokes at 1600 rpm with a Yellowline OST basic homogenizer and mitochondria isolated by  
378 differential centrifugation according to (Frezza et al., 2007).

#### 379 **Molecular cloning**

##### 380 *LETM1 for mass spectrometry experiments*

381 Expression constructs for LETM1-SH were PCR amplified from pVT-U LETM1 (Nowikovsky et  
382 al., 2004) and subcloned into the pTO-SII-HA-GW vector which was a kind gift from M.  
383 Gstaiger (ETH, Zurich). Subcloning was done by Gateway cloning (Invitrogen, Carlsbad, CA).  
384 Plasmid (pTO-SII-HA-GW GFP) expressing N-terminal tagged GFP with Strep-HA tag was a kind

385 gift from A. Bergthaler (CeMM, Vienna). Primers: attB LETM1 forward  
386 5'GGGGACAAGTTTGTACAAAAAAGCAGGCTAGACTGCCATGGCGTCCAT3'

387 , attB LETM1 reverse 5'GGGGACCACTTTGTACAAGAAAGCTGGGTTGCTCTTCACCTCTGCGAC3'.

#### 388 *MICS1 for rescue experiments*

389 The human MICS1 cDNA was amplified by reverse-transcriptase PCR using the forward primer  
390 5'AAGCTTGACCATGTTGGCTGCAAGG3', and the reverse primer with in frame Flag sequence  
391 5'GTCTCTCGAGTTACTTGTTCATCGTCATCCTTGTAACTTTCTTTCTGTTGCCTCC3' and cloned into  
392 the pcDNA3 Plasmid (Sigma Aldrich) using the restriction sites *HindIII* and *XhoI*.

#### 393 *MICS1 for proteoliposomes*

394 Codon optimization of the human MICS1 sequence (UniProtKB: Q9H3K2; GenPept accession  
395 no. NP\_055209.2) was designed using Genscript and increased the Codon Adaptation Index  
396 (CAI) from 0.32 to 0.97. The codon optimized cDNA encoding for human MICS1 protein was  
397 sub-cloned from pUC57 by double digestion and inserted between *HindIII* and *XhoI* restriction  
398 sites of the pH6EX3 expression vector. The resulting recombinant plasmid encodes a 6His-  
399 tagged fusion protein corresponding to the hMICS1 carrying the extra N-terminal sequence  
400 MSPIHSHHHHLVPRGSEA.

#### 401 **Generation of stable LETM1-StrepHA or MICS1-Flag expressing cell lines**

402 Cells were transfected with Turbofect according to the manufacturer instructions; 48 hrs post  
403 transfection the media was changed to selection media as according to the resistance marker  
404 of the plasmid. The concentration of selection antibiotics as listed: hygromycin (260 µg/mL),  
405 blasticidin S (38 µg/mL). After a resistant population of cells was established, cells were

406 maintained in growth media containing: hygromycin (100 µg/mL), blasticidin S (15 µg/mL).

407 For stable MICS1-Flag cells G418 (1 mg/mL) was used in media devoid of FBS and pen/strep.

#### 408 **AP-MS sample preparation**

409 N-terminally tagged GFP or LETM1 inducible HEK293 Flp-In T-Rex were generated as outlined

410 above. Protein expression was induced with doxycycline (1µg/mL) for 24 hrs in standard

411 culture media. Cells were lysed and the bait protein purified by affinity purification (AP) as

412 described (Rudashevskaya et al., 2013). Affinity purification from mitochondria was

413 performed as (Rudashevskaya et al., 2013) with modification. Crudely isolated mitochondria

414 were lysed using 6-aminocaproic acid with protease inhibitors and n-Dodecyl β-D-maltese

415 (2% w/v) and vortexed for 30 min at 4 °C. Lysates were cleared at 15000 ×g, 4 °C for 15 min

416 and the supernatant was quantified by Bradford assay with BSA as standard. Protein

417 complexes were purified from 2 mg crude mitochondrial input with Streptactin (IBA,

418 Göttingen, Germany) beads. Washing steps were performed in scaled volume of AP buffer,

419 thrice with detergent, twice without and then eluted with biotin (Alfa-Aesar, Ward Hill, MA).

420 Protein complexes were reduced, alkylated and digested with trypsin as described

421 (Rudashevskaya et al., 2013). Peptides were desalted and concentrated by reversed-phase

422 tips (Rappsilber et al., 2007) and reconstituted in formic acid (5%) for LC-MS analysis.

#### 423 **Reversed-phase LC-MS data analysis and data filtering**

424 All liquid chromatography mass spectrometry experiments were performed on an Agilent

425 1200 HPLC nanoflow system coupled to a linear trap quadrupole (LTQ) Orbitrap Velos mass

426 spectrometer (ThermoFisher Scientific). Raw data were matched to peptides and proteins

427 using Mascot and Phenyx, with a false discovery rate of 1% at the protein level. CRAPome and

428 SAINT analysis were applied to all AP-MS data. GFP pulldowns were used as controls together

429 with publically-available CRAPome data that used similar sample preparation and MS  
430 methods and instrumentation. Common contaminants and proteins with a frequency greater  
431 than or equal to 0.1 in the CRAPome database were excluded. Proteins with a SAINT score  
432 greater than 0.97 were identified as high confidence interactors.

### 433 **Co-immunoprecipitation**

434 Cells were washed with PBS and harvested in coIP buffer (150 mM NaCl, 50 mM Tris, 2 mM  
435 EDTA, 1% IGEPAL C360, and protease inhibitor tablet without EDTA. Cells lysates were  
436 vortexed, cleared and quantified as described above. Lysates (500 µg or 1 mg) were then  
437 incubated overnight with Streptactin beads or primary antibody as indicated (10 µg). Primary  
438 antibody samples were then incubated for 1 hr at RT with ProtA/G agarose. Beads were then  
439 washed 3 times with coIP buffer then 2 times with PBS and eluted with 1X Laemmli buffer for  
440 SDS-PAGE and immunoblotting.

### 441 **Western blotting: SDS and BN PAGE**

442 SDS PAGE and immunoblotting were performed as in (Austin et al., 2017). Bradford or BCA  
443 assays were performed according to the manufacturer's protocol and blots were quantified  
444 using the BioRad Image Lab (v6.1.0) software. For BNGE, isolated mitochondria were  
445 solubilized with a final concentration of 1% digitonin for 15 min on ice, centrifuged at 27000  
446 ×g for 30 min in a Beckman Optima™ ultracentrifuge and the supernatant (corresponding to  
447 5 µg) with G-250 Sample Additive (0.5 µl) was separated using precasted gels (NativePAGE™  
448 3-12 % Bis-Tris Protein). Unstained Protein Standard NativeMark™ served as a marker.  
449 Protein complexes were transferred onto PVDF membranes overnight using wet blotting at  
450 30 V.

451 **Proliferation assay**

452 Cells were seeded counted manually every 24 hrs by trypan blue exclusion. At least three  
453 independent counts were performed on each sample. Cell numbers were plotted and data  
454 shown as means  $\pm$  SD.

455 **Light scattering assays**

456 Light scattering experiments were adapted from previous protocols (Austin et al., 2017)  
457 Briefly, mitochondria were isolated from HEK293 and HeLa cells as described in (Frezza et al.,  
458 2007) and resuspended in isolation media (200 mM Sucrose, 10 mM Mops-TRIS, 1 mM EGTA-  
459 TRIS, pH:7,4). Antimycin A (5  $\mu$ M) was used at RT to depolarize mitochondria and A123187 (1  
460  $\mu$ M) and EDTA (10  $\mu$ M) to deplete matrix magnesium. Light scattering assays were conducted  
461 in a photometric 96 well plate reader (Varioscan) at RT; KOAc media (180  $\mu$ l), as described in  
462 (Austin et al., 2017) was injected to 200  $\mu$ g mitochondria (total volume 200  $\mu$ l) and  
463 absorbance was detected at OD<sub>540 nm</sub>. Quinine (0.5 mM) served to inhibit the KHE. The  
464 swelling rate was quantified by one phase decay on raw swelling data as shown, K value as  
465 rate constant.

466 **Ca<sup>2+</sup> uptake/release assays**

467 Cells ( $7 \times 10^6$ ) were permeabilized with digitonin (1.25 %) in 400  $\mu$ l permeabilization media  
468 PM1 (KCl (130 mM), Mops-Tris pH 7.4 (10 mM) EGTA-Tris (1 mM), KPi pH.7.4 (1 mM).  
469 Permeabilization was stopped (immediately after 80-90% of the cells had become permeable  
470 to trypan blue) in 600  $\mu$ l PM2 (KCl (130 mM), Mops-Tris pH 7.4 (10 mM), EGTA-Tris (10  $\mu$ M),  
471 KPi pH.7.4 (1 mM), and resuspended in measurement media contained sucrose (250 mM),  
472 MOPS-Tris (10 mM), EGTA-Tris (10  $\mu$ M), KPi 7.4 (1 mM), sodium succinate (5 mM) rotenone

473 (2  $\mu\text{M}$ ), sodium succinate (5 mM) to energize CII and rotenone (2  $\mu\text{M}$ ) to block CI. CGP37157  
474 (2  $\mu\text{M}$ ) served to inhibit NCLX, and when indicated thapsigargin (1  $\mu\text{M}$ ) to block SERCA.  
475 Calcium Green-5N (0.24  $\mu\text{M}$ ) was used to record extramitochondrial  $\text{Ca}^{2+}$ , TMRM (0.33  $\mu\text{M}$ )  
476 to measure the membrane potential. A bolus of  $\text{CaCl}_2$  (10  $\mu\text{M}$ ) was applied to initiate  $\text{Ca}^{2+}$   
477 uptake. MCU was inhibited by addition of RR (0.2  $\mu\text{M}$ ), which induced  $\text{Ca}^{2+}$  release. FCCP (2  
478  $\mu\text{M}$ ) or alamethicin (2.5  $\mu\text{M}$ ) was added to induce the maximal release of total  $\text{Ca}^{2+}$  at the end  
479 of the measurement. The LS55 spectrofluorometer 211 (Perkin Elmer) was used with the  
480 following parameters:  $\text{Ca}^{2+}$  green-5N:  $\lambda_{\text{ex}} = 505$  nm,  $\lambda_{\text{em}} = 530$  nm, slit width: Ex-2.5 nm, Em-  
481 2.5 nm; TMRM:  $\lambda_{\text{ex}} = 546$  nm,  $\lambda_{\text{em}} = 590$  nm, slit width: 2.5 nm.

#### 482 **Calcium Retention Capacity experiment**

483 The measurements were performed in media as described for  $\text{Ca}^{2+}$  uptake release assay,  
484 containing Calcium Green-5N and when indicated thapsigargin (1  $\mu\text{M}$ ) CsA (1  $\mu\text{M}$ ) and/ or  
485 CGP37157 (1  $\mu\text{M}$ ).  $\text{CaCl}_2$  pulses (5  $\mu\text{M}$ ) were added sequentially until the opening of PTP  
486 occurred. Measurements were performed using the LS55 spectrofluorometer 211 (Perkin  
487 Elmer) with the same parameters as for  $\text{Ca}^{2+}$  uptake release.

#### 488 **Seahorse Mito Stress assay**

489 Extracellular flux analyses were performed with the Agilent Seahorse XF24 Extracellular flux  
490 analyser as outlined in (Wilfinger et al., 2016), with minor modifications to inhibitor  
491 concentration, oligomycin (0.5  $\mu\text{M}$ ) and FCCP (0.2  $\mu\text{M}$ ). Carbon source is indicated in the  
492 figure legends, either (glucose 25 mM) or galactose (10 mM), all media were supplemented  
493 with sodium pyruvate (1 mM).

#### 494 **Transmission electron microscopy**

495 Cells were fixed in glutaraldehyde (5%) phosphate buffer (0.1 M) (Sigma–Aldrich, Vienna,  
496 Austria), pH 7.2, at 4 °C for 2 hrs. Subsequently, samples were post-fixed in 1% osmium  
497 tetroxide in the same buffer at 4 °C for 1 hr. After dehydration in an alcohol gradient series  
498 and propylene oxide, the tissue samples were embedded in glycid ether 100. Ultrathin  
499 sections were cut on a Leica ultramicrotome (Leica Ultracut S, Vienna, Austria), stained with  
500 uranyl acetate and lead citrate and examined with a Zeiss TEM 900 electron microscope (Carl  
501 Zeiss, Oberkochen, Germany) operated at 80 kV.

## 502 **Live cell imaging**

503 For confocal microscopy 5 x 10<sup>4</sup> cells/well were seeded onto poly-L-lysine coated  $\mu$ -Slide 8  
504 well plates (Ibidi, #80826). The next day mitochondria were loaded with MitoTracker™ Green  
505 FM (50 nM) for 30 minutes and then changed to fresh medium before they were monitored  
506 under 5 % CO<sub>2</sub> at 37 °C using a LSM880 microscope with Plan-Apochromat 63x/1.40 Oil DIC  
507 M27 lens. MTG was excited at a wavelength of 488 nm and images were processed in Adobe  
508 Photoshop CS2.

## 509 **Over-expression, purification and reconstitution in proteoliposomes of MICS1 for Ca<sup>2+</sup>** 510 **transport assays**

### 511 *Expression of MICS1 protein*

512 To produce the 6His- MICS1 recombinant protein, *E. coli* Rosetta cells (Novagen) were  
513 transformed with the pH6EX3-hMICS1 construct. Selection of transformed colonies was  
514 performed on LB-agar plates added with ampicillin (100  $\mu$ g/mL) and chloramphenicol (34  
515  $\mu$ g/mL). A colony was inoculated and cultured overnight at 37 °C under rotary shaking (160  
516 rpm). The day after, the culture was diluted 1:20 in fresh medium added with the specific

517 antibiotics. When the optical density measured at OD<sub>600 nm</sub> wavelength was 0.8-1, different  
518 IPTG concentrations (from 0.1 to 1 mM) were tested to induce protein expression except for  
519 one aliquot, grown in absence of inducer (negative control). The cultures were continued for  
520 up to 6 hours at 28 °C or 37 °C at 160 rpm. Every two hours, aliquots were collected and  
521 centrifuged at 3000 ×g, and at 4 °C for 10 minutes; the pellets were stored at -20 °C. A bacterial  
522 pellet aliquot, after thawing, was dissolved in a resuspension buffer (20 mM Hepes Tris, 200  
523 mM NaCl pH 7.5) added with protease inhibitor cocktail according to manufacturer  
524 instructions. The bacterial suspensions were sonicated in an ice bath for 10 minutes (pulse of  
525 1 second on, and 1 second off) at 40 Watt, using a Vibracell VCX-130 sonifier. The insoluble  
526 cell fractions were analyzed by SDS-PAGE and western blotting.

#### 527 *Purification of hMICS1*

528 hMICS1, over-expressed in *E. coli*, was purified by Ni-chelating chromatography. In brief, the  
529 insoluble fraction of bacterial cell lysates was firstly washed with a buffer containing Tris-HCl  
530 pH 8.0 (0.1 M). After centrifugation step (12000 ×g for 5 min at 4 °C), pellet was resuspended  
531 with 100 mM 1,4-dithioerythritol (DTE) and then solubilized with a buffer containing urea (3.5  
532 M), sarkosyl (0.8%), NaCl (100 mM), glycerol (5%), Tris HCl pH 8.0 (10 mM). After  
533 solubilization, the sample was centrifuged at 12000 ×g for 10 min at 4 °C and the supernatant  
534 was applied onto a column filled with 2 mL His select nickel affinity gel (0.5 cm diameter, 2.5  
535 cm height) pre-conditioned with 8 mL of a buffer containing sarkosyl (0.1%), NaCl (200 mM),  
536 glycerol (10%), Tris HCl pH 8.0 (20 mM). Then, 5 mL of a buffer containing Tris HCl pH 8.0 (20  
537 mM), glycerol (10%), NaCl (200 mM), n-Dodecyl β-D-maltoside (0.1%) and DTE (5 mM) was  
538 used to wash the column removing unbound proteins. In order to increase the purity of the  
539 recovered MICS1, another washing step was performed using 3 mL of the same above-



540 described buffer added with 10 mM imidazole. Finally, MICS1 was eluted in 5 fractions of 1  
541 mL, using the same above-described buffer added with 50 mM imidazole. The purified protein  
542 was eluted in a peak of 2.5 mL. The eluted protein was subjected to a buffer change for  
543 imidazole and Na<sup>+</sup> removal, using a PD-10 column pre-conditioned with a desalt buffer  
544 composed of Tris HCl pH 8.0 (20 mM), glycerol (10%), n-Dodecyl β-D-maltoside (0.1%) and  
545 DTE (10 mM): 2.5 mL of the purified protein were loaded onto the PD10 column and collected  
546 in 3.5 mL of desalt buffer.

#### 547 *Reconstitution in proteoliposomes of the purified hMICS1*

548 The desalted hMICS1 was reconstituted by removing detergent from mixed micelles of  
549 detergent, protein and phospholipids using the batch wise method previously described for  
550 other membrane proteins (Cosco et al., 2020), with some modifications to increase the  
551 protein/phospholipid ratio required for fluorometric measurements (Scalise et al., 2020). The  
552 initial mixture contained: 25 μg of purified protein, 50 μL of 10% C<sub>12</sub>E<sub>8</sub>, 50 μL of 10% egg yolk  
553 phospholipids (w/v) in the form of liposomes prepared as previously described (Scalise et al.,  
554 2018), 20 mM Tris HCl pH 7.0, except where differently indicated, 10 μM of Calcium Green-  
555 5N or 20 μM pyranine, in a final volume of 700 μL. The detergent was removed by incubating  
556 the reconstitution mixture with 0.5 g of the hydrophobic resin Amberlite XAD-4 for 40 min  
557 under rotatory stirring at room temperature.

#### 558 *Cation transport measurements by spectrofluorometric assays*

559 The Ca<sup>2+</sup> flux or the intraliposomal pH changes were monitored by measuring the  
560 fluorescence emission of Calcium Green-5N or pyranine, respectively included inside the  
561 proteoliposomes. After reconstitution, 600 μL of proteoliposomes was passed through a  
562 Sephadex G-75 column, pre-equilibrated with Tris HCl pH 7.0 (20 mM), except where

563 differently indicated. Then, 200  $\mu$ L proteoliposomes were diluted in 3 mL of the same buffer  
564 and incubated for 10 min in the dark prior to measurements. To start the transport assay,  
565  $\text{CaCl}_2$  (7 mM) buffered at pH 7.0, except where differently indicated, was added to  
566 proteoliposomes; the uptake of  $\text{Ca}^{2+}$  or the efflux of  $\text{H}^+$  was measured as an increase of  
567 Calcium Green-5N or pyranine fluorescence, respectively. As a control, the same  
568 measurements were performed using liposomes, i.e., vesicles without reconstituted hMICS1.  
569 The measurements were performed in the fluorescence spectrometer (LS55) from Perkin  
570 Elmer under rotatory stirring. The fluorescence was measured following time drive acquisition  
571 protocol with  $\lambda$  excitation=506 nm and  $\lambda$  emission=532nm (slit 5/5) for Calcium Green-5N and  
572  $\lambda$  excitation=450 nm and  $\lambda$  emission=520nm (slit 5/5) for pyranine.

### 573 **Statistical analysis**

574 All statistical analyses were done in GraphPad (La Jolla, CA) Prism v6 for Windows. Bar graphs  
575 were generated with GraphPad Prism. Tests and individual  $p$  values as indicated in figure  
576 legends. The data are presented as mean  $\pm$  SD unless specified.

577

### 578 **Figure legend**

#### 579 **Figure 1 LETM1 and MICS1 interact**

580 **(A)** LETM1 interactome as determined by affinity purification mass spectrometry (AP-MS). All  
581 high confidence interaction partners of LETM1 are shown as nodes. Node color indicates  
582 SAINT score, a probability-based measure of interaction confidence. Data are from a single  
583 MS experiment. See also **Figure1–figure supplement 1 (B)** Co-immunoprecipitation of MICS1  
584 and LETM1 protein in tandem. Mitochondria were crudely isolated from HEK293 cells and

585 used for immunoprecipitation. The input represents the mitochondrial crude lysate used as  
586 input for the co-IP, LETM1 was immunoprecipitated (left panel, IP:LETM1) using a LETM1  
587 polyclonal antibody and Protein A/G agarose beads (ProtA/G). ProtA/G beads alone were  
588 used as a negative control for binding, immunoprecipitates were immunoblotted (IB) for the  
589 indicated proteins to demonstrate interaction. Prohibitin was used as a control to illustrate  
590 no nonspecific binding of inner mitochondrial membrane proteins complexes. The right panel  
591 illustrates the converse experiment, MICS1 was precipitated (right panel, IP: MICS1) using a  
592 MICS1 polyclonal antibody. **(C)** Native immunoblot of LETM1 (left) and MICS1 (right) show  
593 that both proteins can be found in protein complexes of the same size (arrows), MICS1  
594 additionally resides in other protein complexes. **(D)** Immunoblot analysis of LETM1 and MICS1  
595 expression on conditions of reduced FBS (0.5%) in culture media. Mitochondrial complex III  
596 integral subunit UQCRC2 is used as loading control.

## 597 **Figure 2 MICS1KD decreases LETM1 and mitochondrial bioenergetics**

598 **(A)** Western blot analysis of LETM1 and MICS1 in HEK293 MICS1WT cell with scramble shRNA  
599 (scr) or two different MICS1 knockdowns (KD#1 or KD#2). HSP60 served as a loading control.  
600 **(B)** Proliferation curve of MICS1WT (WT) with a scrambled construct compared to MICS1KD  
601 cells (KD) over 4 days using a trypan blue exclusion assay to count cells. Data are means  $\pm$  SEM  
602 (n=3), at 96h statistical analysis using an unpaired student's t-test (\*\*\*) $p < 0.001$ . **(C-F)** Cellular  
603 bioenergetics of MICS1KD cells in various nutrient conditions. Oxygen consumption rate of  
604 WT cells with a scrambled control ("WT") and MICS1KD#1 cells grown in **(C)** 25 mM glucose,  
605 **(E)** 10 mM galactose for 24 hours before measurement. Data are representative of at least 3  
606 independent experiments. Shown are mean data of triplicate measurements  $\pm$  SEM.  
607 Inhibitors as indicated: A- oligomycin (0.5  $\mu$ M), B & C- FCCP (0.2  $\mu$ M each), D- antimycin

608 A/rotenone (0.5  $\mu$ M). **(D & F)** Bar charts of XF experiment traces (C & E), data are means of  
609 multiple time points after experiment start or drug addition of at least three independent  
610 experiments  $\pm$  SEM. (n=3). Statistical analysis using an unpaired student's t-test (\*\* $p$ <0.01,  
611 \*\*\* $p$ <0.001).

### 612 **Figure 3 MICS1KO causes mitochondrial matrix swelling and cristae disorganization**

613 **(A)** Western blot analysis of MICS1 in control and targeted HeLa and HEK293 clones, HSP60  
614 served as loading control. **(B)** Proliferation assay of HEK293 cells in function of MICS1. Graph  
615 shows the mean of three individual counts, Two-way ANOVA with Dunnett's multiple  
616 comparisons test performed against MICS1WT \* $p$ =0.0155. **(C)** Live imaging of HEK293  
617 MICS1WT and KO cells stained with MitoTracker Green FM. Bars: 10  $\mu$ m **(D)** Alteration of the  
618 mitochondrial ultrastructure shown by transmission electron microscopy, red arrow pointing  
619 to dilated matrix. Wider mitochondria in middle and right panel compared to controls, a  
620 middle panel showing the strongest phenotype of matrix width and cristae forms. **(E)** Isolated  
621 mitochondria from three independent replicates of HEK293 MICS1WT and MICS1KO#1 (#1)  
622 and KO#2 (#2) were analyzed by immunoblotting using the indicated antibodies, HSP60 and  
623 TOM40 served as mitochondrial loading controls. **(F)** Densitometric analysis of the bands in  
624 (E) normalized to loading control, bar graph of three individual counts, One-way ANOVA with  
625 Bonferroni's multiple comparisons test performed against MICS1WT \* $p$ <0.05, \*\* $p$ <0.008,  
626 Two-way ANOVA with Bonferroni's multiple comparisons test performed for the OPA1  
627 statistics against MICS1WT, \*\*\* $p$ =0.0009, \*\*\*\* $p$ <0.0001.

### 628 **Figure 4 MICS1 and LETM1 are involved in mitochondrial KHE activity**

629 KOAc-induced swelling was measured in mitochondria derived from HEK293 MICS1WT,  
630 MICS1KO and MICS1KO cells stably re-expressing MICS1WT **(A-B)**, HeLa MICS1WT and

631 MICS1KO **(C-D)** and HeLa LETM1 scramble and LETM1 KD **(E-F)** cells. MICS1WT: black traces,  
632 MICS1KO: red traces, MICS1KO + MICS1WT: blue traces, LETM1scr: black trace, LETM1KD:  
633 green trace. **(B)** Quantification of swelling amplitudes from independent experiments (n=3)  
634 HEK293 MICS1WT (black bar,  $100 \pm 19.71$ ) and HEK293 MICS1KO (red bar,  $48.08 \pm 11.906$ ).  
635 Complementation of MICS1KO with re-expression of *MICS1WT* restored swelling rates (blue  
636 bar,  $90.55 \pm 12.93$ ). **(D)** Similar differences in swelling capacities were obtained between HeLa  
637 MICS1WT (black bar;  $100 \pm 9.47$ ) and HeLa MICS1KO (red bar;  $63.48 \pm 8.60$ ). Lower basal  
638 optical density indicates swollen matrix prior KOAc addition; Inhibition of KHE with quinine in  
639 HEK293 cells: WT grey bar,  $18.14 \pm 21.02$ ; KO#1 pink bar,  $9.33 \pm 28.17$ ; MICS1KO+MICS1,  $15.79$   
640  $\pm 10.04$ . Statistical analysis: One-Way ANOVA with Bonferroni correction (\*p < 0.05, \*\*p < 0.01,  
641 \*\*\*p < 0.001). See also **Figure 4–figure supplement 1**.

#### 642 **Figure 5 MICS1 controls Na<sup>+</sup>-independent Ca<sup>2+</sup> release**

643 Ca<sup>2+</sup> uptake/release dynamics are shown as extramitochondrial Ca<sup>2+</sup> changes of fluorescence  
644 intensities of Calcium Green 5N (Ca<sup>2+</sup> 5N) (0.24  $\mu$ M) **(A-L and P-Q)** and membrane potential  
645 as change of fluorescence intensities of TMRM (330 nM) **(M-N)** corresponding to the  
646 measurement of Ca<sup>2+</sup> fluxes in **(K)**. Experiments were performed using permeabilized HEK293  
647 MICS1WT, MICS1KO (KO#1, KO#2) **(A-D)** and **(G-R)**, MICS1KO#1 + MICS1WT cells was included  
648 in **(A-B)**, and HEK293 LETM1 scr and LETM1KD cells **(E-F)** in presence of CGP37157 (2  $\mu$ M).  
649 Ca<sup>2+</sup> (10  $\mu$ M), RR (0.2  $\mu$ M) and FCCP (2  $\mu$ M) or alamethicin (2.5  $\mu$ M) were added when  
650 indicated. CsA was added two minutes before measurements in **(G-J and Q-R)**, nigericin was  
651 added 1 min before measurements in absence of thapsigargin or after Ca<sup>2+</sup> uptake in  
652 thapsigargin experiments to prevent slowed Ca<sup>2+</sup> uptake dynamics in **(I-J)**, thapsigargin (1  $\mu$ M)  
653 was added as indicated in **K-R**, and ADP as indicated in **(Q-R)**. Quantification of Ca<sup>2+</sup> release

654 rates from independent experiments (n=3) (t: 300-920 s) and statistical analysis: One-Way  
655 ANOVA with Bonferroni correction (\*p <0.05, \*\*p <0.01, \*\*\*p <0.001, \*\*\*\*p <0.0001). See  
656 also **Figure 5–figure supplement 1** for quantification of Ca<sup>2+</sup> uptake. Quantification of TMRM  
657 performed with unpaired two-sided t-test (Welsh correction), \*p <0.05. **(O-P)** CRCs showing  
658 that absence of MICS1 supersensitizes mitochondria to Ca<sup>2+</sup>-induced PTP opening by  
659 thapsigargin. See also **Figure 5–figure supplement 2** for CRCs. In absence of thapsigargin.  
660 Permeabilized HEK293 MICS1WT **(O)** and MICS1KO#1 **(P)** cells exposed or not to CsA were  
661 subjected to sequential Ca<sup>2+</sup> bolus of 5 μM Ca<sup>2+</sup> and fluorescence intensity was recorded. **(Q-**  
662 **R)** Thapsigargin-dependent Ca<sup>2+</sup> uptake/release experiments repeated in presence of CsA and  
663 ADP in MICS1WT and MICS1KO#1 and KO#2 showing the suppression of Ca<sup>2+</sup> release,  
664 quantifications using One-Way ANOVA with Bonferroni correction.

#### 665 **Figure 6 MICS1 proteoliposomes mediate Ca<sup>2+</sup> and Ca<sup>2+</sup>-dependent H<sup>+</sup> transport**

666 **(A)** Sketch illustrating the reconstitution of hMICS1 (red) in proteoliposomes and the empty  
667 liposomes (blue) for transport measurements. **(B)** Western blot analysis of purified and  
668 reconstituted hMICS1 for evaluating the incorporation of hMICS1 into proteoliposomes  
669 prepared as described in materials and methods. Transport of Ca<sup>2+</sup> **(C-E)** or H<sup>+</sup> **(F)** by hMICS1  
670 reconstituted in proteoliposomes. Purified hMICS1 was reconstituted in proteoliposomes  
671 containing 10 μM Calcium Green 5N at the pH indicated in the panels **(C-E)** or 20 μM pyranine  
672 at pH 7.0 **(F)**. After reconstitution, the fluorescence measurement was started by diluting 200  
673 μL proteoliposomes (red trace) up to 3 mL with transport buffer prepared as described in  
674 materials and methods at the indicated pH **(C)** or at pH 7.0 **(D)**. After 100 sec, as indicated by  
675 the arrow, 7 mM Ca<sup>2+</sup> was added to the sample and fluorescence change was recorded. As a  
676 control, the same measurement was performed diluting 200 μL liposomes (without

677 incorporated protein, blue trace) up to 3 mL with the same transport buffer. The fluorescence  
678 intensity is indicated as Arbitrary Units (AU). Results are representative of three independent  
679 experiments. See also **Figure 6–figure supplement 1** for MICS1 optimization, induction and  
680 structure overview.

681

## 682 **Acknowledgement**

683 We thank Dr Martha Giacomello for constructive discussion and experimental support and Dr  
684 Paolo Bernardi for critical reading of the manuscript. This work was supported by the Doc  
685 fellowship from the Austrian Academy of Science ÖAW to SA and the Austrian Science Funds  
686 FWF research project grants P-314717 and P-29077 to KN.

687

## 688 **Author contributions**

689 KN conceived the study and supervised the experimental work. SA performed the  
690 interactome, co-immunoprecipitation, bioenergetics, generated LETM1 and MICS1  
691 knockdowns and analysed the data. RM performed  $K^+$ ,  $Ca^{2+}$  flux, CRC and delta psi  
692 measurements and data analysis, SM conducted immunofluorescence, cell biological and  
693 protein analysis, MS and MG generated *E. coli* strains, purified and reconstituted proteins and  
694 performed cell-free flux measurements, CP performed BNGE and TB LETM1 SDS-PAGE. KB  
695 designed and supervised mass spectrometry analysis, KP and DV participated in method  
696 development and running of LC-MS instrumentation, ND conducted TEM, CI designed the cell-  
697 free study, KN, SA and CI wrote the manuscript.

698

## 699 **Declaration of interests**

700 The authors declare no competing interest.

701

702

## 703 **References**

704 Austin, S., and Nowikovsky, K. (2019). LETM1: Essential for Mitochondrial Biology and Cation  
705 Homeostasis? Trends in biochemical sciences *44*, 648-658.  
706 Austin, S., and Nowikovsky, K. (2021). Mitochondrial osmoregulation in evolution, cation  
707 transport and metabolism. Biochimica et biophysica acta Bioenergetics *1862*, 148368.



708 Austin, S., Tavakoli, M., Pfeiffer, C., Seifert, J., Mattarei, A., De Stefani, D., Zoratti, M., and  
709 Nowikovsky, K. (2017). LETM1-Mediated K(+) and Na(+) Homeostasis Regulates  
710 Mitochondrial Ca(2+) Efflux. *Frontiers in physiology* 8, 839.

711 Basso, E., Petronilli, V., Forte, M.A., and Bernardi, P. (2008). Phosphate is essential for  
712 inhibition of the mitochondrial permeability transition pore by cyclosporin A and by  
713 cyclophilin D ablation. *The Journal of biological chemistry* 283, 26307-26311.

714 Beghi, E., and Giussani, G. (2018). Aging and the Epidemiology of Epilepsy.  
715 *Neuroepidemiology* 51, 216-223.

716 Bernardi, P. (1999). Mitochondrial transport of cations: channels, exchangers, and  
717 permeability transition. *Physiological reviews* 79, 1127-1155.

718 Carafoli, E., Tiozzo, R., Lugli, G., Crovetti, F., and Kratzing, C. (1974). The release of calcium  
719 from heart mitochondria by sodium. *Journal of molecular and cellular cardiology* 6, 361-371.

720 Carrara, G., Saraiva, N., Gubser, C., Johnson, B.F., and Smith, G.L. (2012). Six-transmembrane  
721 topology for Golgi anti-apoptotic protein (GAAP) and Bax inhibitor 1 (BI-1) provides model for  
722 the transmembrane Bax inhibitor-containing motif (TMBIM) family. *The Journal of biological*  
723 *chemistry* 287, 15896-15905.

724 Cosco, J., Scalise, M., Colas, C., Galluccio, M., Martini, R., Rovella, F., Mazza, T., Ecker, G.F.,  
725 and Indiveri, C. (2020). ATP modulates SLC7A5 (LAT1) synergistically with cholesterol.  
726 *Scientific reports* 10, 16738.

727 De Stefani, D., Rizzuto, R., and Pozzan, T. (2016). Enjoy the Trip: Calcium in Mitochondria Back  
728 and Forth. *Annual review of biochemistry* 85, 161-192.

729 Del Dotto, V., Mishra, P., Vidoni, S., Fogazza, M., Maresca, A., Caporali, L., McCaffery, J.M.,  
730 Cappelletti, M., Baruffini, E., Lenaers, G., *et al.* (2017). OPA1 Isoforms in the Hierarchical  
731 Organization of Mitochondrial Functions. *Cell reports* 19, 2557-2571.

732 Doonan, P.J., Chandramoorthy, H.C., Hoffman, N.E., Zhang, X., Cardenas, C., Shanmughapriya,  
733 S., Rajan, S., Vallem, S., Chen, X., Foskett, J.K., *et al.* (2014). LETM1-dependent mitochondrial  
734 Ca<sup>2+</sup> flux modulates cellular bioenergetics and proliferation. *FASEB journal : official*  
735 *publication of the Federation of American Societies for Experimental Biology* 28, 4936-4949.

736 Endele, S., Fuhry, M., Pak, S.J., Zabel, B.U., and Winterpacht, A. (1999). LETM1, a novel gene  
737 encoding a putative EF-hand Ca(2+)-binding protein, flanks the Wolf-Hirschhorn syndrome  
738 (WHS) critical region and is deleted in most WHS patients. *Genomics* 60, 218-225.

739 Frezza, C., Cipolat, S., and Scorrano, L. (2007). Organelle isolation: functional mitochondria  
740 from mouse liver, muscle and cultured fibroblasts. *Nature protocols* 2, 287-295.

741 Galluccio, M., Pingitore, P., Scalise, M., and Indiveri, C. (2013). Cloning, large scale over-  
742 expression in *E. coli* and purification of the components of the human LAT 1 (SLC7A5) amino  
743 acid transporter. *Protein J* 32, 442-448.

744 Giorgi, C., Marchi, S., and Pinton, P. (2018). The machineries, regulation and cellular functions  
745 of mitochondrial calcium. *Nature reviews Molecular cell biology* 19, 713-730.

746 Guo, G., Xu, M., Chang, Y., Luyten, T., Seitaj, B., Liu, W., Zhu, P., Bultynck, G., Shi, L., Quick, M.,  
747 *et al.* (2019). Ion and pH Sensitivity of a TMBIM Ca(2+) Channel. *Structure* 27, 1013-1021  
748 e1013.

749 Hasegawa, A., and van der Bliek, A.M. (2007). Inverse correlation between expression of the  
750 Wolf Hirschhorn candidate gene *Letm1* and mitochondrial volume in *C. elegans* and in  
751 mammalian cells. *Hum Mol Genet* 16, 2061-2071.

752 Hashimi, H., McDonald, L., Stribrna, E., and Lukes, J. (2013). Trypanosome *Letm1* protein is  
753 essential for mitochondrial potassium homeostasis. *The Journal of biological chemistry* 288,  
754 26914-26925.

755 Hung, Y.P., Albeck, J.G., Tantama, M., and Yellen, G. (2011). Imaging cytosolic NADH-NAD(+)  
756 redox state with a genetically encoded fluorescent biosensor. *Cell metabolism* *14*, 545-554.

757 Jiang, D., Zhao, L., and Clapham, D.E. (2009). Genome-wide RNAi screen identifies Letm1 as a  
758 mitochondrial Ca<sup>2+</sup>/H<sup>+</sup> antiporter. *Science* *326*, 144-147.

759 Jiang, D., Zhao, L., Clish, C.B., and Clapham, D.E. (2013). Letm1, the mitochondrial Ca<sup>2+</sup>/H<sup>+</sup>  
760 antiporter, is essential for normal glucose metabolism and alters brain function in Wolf-  
761 Hirschhorn syndrome. *Proceedings of the National Academy of Sciences of the United States*  
762 *of America* *110*, E2249-2254.

763 Jumper, J., Evans, R., Pritzel, A., Green, T., Figurnov, M., Ronneberger, O., Tunyasuvunakool,  
764 K., Bates, R., Zidek, A., Potapenko, A., *et al.* (2021). Highly accurate protein structure  
765 prediction with AlphaFold. *Nature*.

766 Kim, H.K., Lee, G.H., Bhattarai, K.R., Lee, M.S., Back, S.H., Kim, H.R., and Chae, H.J. (2021).  
767 TMBIM6 (transmembrane BAX inhibitor motif containing 6) enhances autophagy through  
768 regulation of lysosomal calcium. *Autophagy* *17*, 761-778.

769 Korge, P., and Weiss, J.N. (1999). Thapsigargin directly induces the mitochondrial permeability  
770 transition. *European journal of biochemistry* *265*, 273-280.

771 Li, S., Wang, L., Berman, M., Kong, Y.Y., and Dorf, M.E. (2011). Mapping a dynamic innate  
772 immunity protein interaction network regulating type I interferon production. *Immunity* *35*,  
773 426-440.

774 Lisak, D.A., Schacht, T., Enders, V., Habicht, J., Kiviluoto, S., Schneider, J., Henke, N., Bultynck,  
775 G., and Methner, A. (2015). The transmembrane Bax inhibitor motif (TMBIM) containing  
776 protein family: Tissue expression, intracellular localization and effects on the ER CA(2)(+)-  
777 filling state. *Biochimica et biophysica acta* *1853*, 2104-2114.

778 Liu, Q. (2017). TMBIM-mediated Ca(2+) homeostasis and cell death. *Biochimica et biophysica*  
779 *acta Molecular cell research* 1864, 850-857.

780 Luongo, T.S., Lambert, J.P., Gross, P., Nwokedi, M., Lombardi, A.A., Shanmughapriya, S.,  
781 Carpenter, A.C., Kolmetzky, D., Gao, E., van Berlo, J.H., *et al.* (2017). The mitochondrial  
782 Na(+)/Ca(2+) exchanger is essential for Ca(2+) homeostasis and viability. *Nature* 545, 93-97.

783 McQuibban, A.G., Joza, N., Megighian, A., Scorzeto, M., Zanini, D., Reipert, S., Richter, C.,  
784 Schweyen, R.J., and Nowikovsky, K. (2010). A *Drosophila* mutant of LETM1, a candidate gene  
785 for seizures in Wolf-Hirschhorn syndrome. *Human molecular genetics* 19, 987-1000.

786 Mitchell, P. (1966). Chemiosmotic coupling in oxidative and photosynthetic phosphorylation.  
787 *Biological reviews of the Cambridge Philosophical Society* 41, 445-502.

788 Nowikovsky, K., and Bernardi, P. (2014). LETM1 in mitochondrial cation transport. *Frontiers*  
789 *in physiology* 5, 83.

790 Nowikovsky, K., Froschauer, E.M., Zsurka, G., Samaj, J., Reipert, S., Kolisek, M., Wiesenberger,  
791 G., and Schweyen, R.J. (2004). The LETM1/YOL027 gene family encodes a factor of the  
792 mitochondrial K+ homeostasis with a potential role in the Wolf-Hirschhorn syndrome. *The*  
793 *Journal of biological chemistry* 279, 30307-30315.

794 Nowikovsky, K., Pozzan, T., Rizzuto, R., Scorrano, L., and Bernardi, P. (2012). Perspectives on:  
795 SGP symposium on mitochondrial physiology and medicine: the pathophysiology of LETM1.  
796 *The Journal of general physiology* 139, 445-454.

797 Nowikovsky, K., Reipert, S., Devenish, R.J., and Schweyen, R.J. (2007). Mdm38 protein  
798 depletion causes loss of mitochondrial K+/H+ exchange activity, osmotic swelling and  
799 mitophagy. *Cell death and differentiation* 14, 1647-1656.

800 Oka, T., Sayano, T., Tamai, S., Yokota, S., Kato, H., Fujii, G., and Mihara, K. (2008). Identification  
801 of a novel protein MICS1 that is involved in maintenance of mitochondrial morphology and  
802 apoptotic release of cytochrome c. *Molecular biology of the cell* *19*, 2597-2608.

803 Olichon, A., Baricault, L., Gas, N., Guillou, E., Valette, A., Belenguer, P., and Lenaers, G. (2003).  
804 Loss of OPA1 perturbs the mitochondrial inner membrane structure and integrity, leading  
805 to cytochrome c release and apoptosis. *The Journal of biological chemistry* *278*, 7743-7746.

806 Pallafacchina, G., Zanin, S., and Rizzuto, R. (2018). Recent advances in the molecular  
807 mechanism of mitochondrial calcium uptake. *F1000Research* *7*.

808 Rappsilber, J., Mann, M., and Ishihama, Y. (2007). Protocol for micro-purification, enrichment,  
809 pre-fractionation and storage of peptides for proteomics using StageTips. *Nature protocols* *2*,  
810 1896-1906.

811 Rojas-Rivera, D., and Hetz, C. (2015). TMBIM protein family: ancestral regulators of cell death.  
812 *Oncogene* *34*, 269-280.

813 Rudashevskaya, E.L., Sacco, R., Kratochwill, K., Huber, M.L., Gstaiger, M., Superti-Furga, G.,  
814 and Bennett, K.L. (2013). A method to resolve the composition of heterogeneous affinity-  
815 purified protein complexes assembled around a common protein by chemical cross-linking,  
816 gel electrophoresis and mass spectrometry. *Nature protocols* *8*, 75-97.

817 Sambri, I., Massa, F., Gullo, F., Meneghini, S., Cassina, L., Carraro, M., Dina, G., Quattrini, A.,  
818 Patanella, L., Carissimo, A., *et al.* (2020). Impaired flickering of the permeability transition  
819 pore causes SPG7 spastic paraplegia. *EBioMedicine* *61*, 103050.

820 Sancak, Y., Markhard, A.L., Kitami, T., Kovacs-Bogdan, E., Kamer, K.J., Udeshi, N.D., Carr, S.A.,  
821 Chaudhuri, D., Clapham, D.E., Li, A.A., *et al.* (2013). EMRE is an essential component of the  
822 mitochondrial calcium uniporter complex. *Science* *342*, 1379-1382.

823 Scalise, M., Mazza, T., Pappacoda, G., Pochini, L., Cosco, J., Rovella, F., and Indiveri, C. (2020).  
824 The Human SLC1A5 Neutral Amino Acid Transporter Catalyzes a pH-Dependent  
825 Glutamate/Glutamine Antiport, as Well. *Front Cell Dev Biol* 8, 603.

826 Scalise, M., Pochini, L., Console, L., Pappacoda, G., Pingitore, P., Hedfalk, K., and Indiveri, C.  
827 (2018). Cys Site-Directed Mutagenesis of the Human SLC1A5 (ASCT2) Transporter:  
828 Structure/Function Relationships and Crucial Role of Cys467 for Redox Sensing and Glutamine  
829 Transport. *Int J Mol Sci* 19.

830 Seitaj, B., Maull, F., Zhang, L., Wullner, V., Wolf, C., Schippers, P., La Rovere, R., Distler, U.,  
831 Tenzer, S., Parys, J.B., *et al.* (2020). Transmembrane BAX Inhibitor-1 Motif Containing Protein  
832 5 (TMBIM5) Sustains Mitochondrial Structure, Shape, and Function by Impacting the  
833 Mitochondrial Protein Synthesis Machinery. *Cells* 9.

834 Shao, J., Fu, Z., Ji, Y., Guan, X., Guo, S., Ding, Z., Yang, X., Cong, Y., and Shen, Y. (2016). Leucine  
835 zipper-EF-hand containing transmembrane protein 1 (LETM1) forms a Ca(2+)/H(+) antiporter.  
836 *Scientific reports* 6, 34174.

837 Urbani, A., Prosdocimi, E., Carrer, A., Checchetto, V., and Szabo, I. (2020). Mitochondrial Ion  
838 Channels of the Inner Membrane and Their Regulation in Cell Death Signaling. *Frontiers in cell*  
839 *and developmental biology* 8, 620081.

840 Wilfinger, N., Austin, S., Scheiber-Mojdekar, B., Berger, W., Reipert, S., Prashberger, M.,  
841 Paur, J., Trondl, R., Keppler, B.K., Zielinski, C.C., *et al.* (2016). Novel p53-dependent anticancer  
842 strategy by targeting iron signaling and BNIP3L-induced mitophagy. *Oncotarget* 7, 1242-1261.

843

**Figure 1**

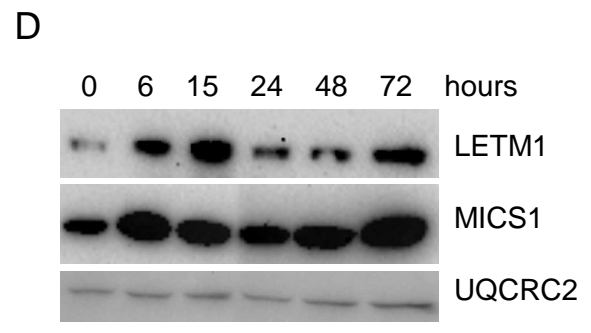
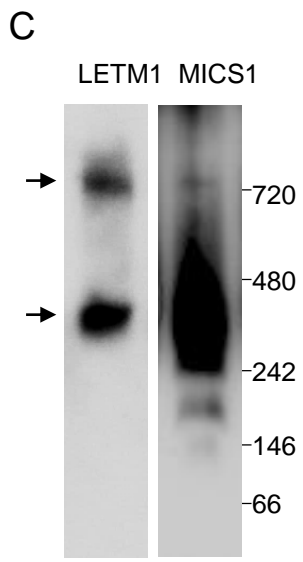
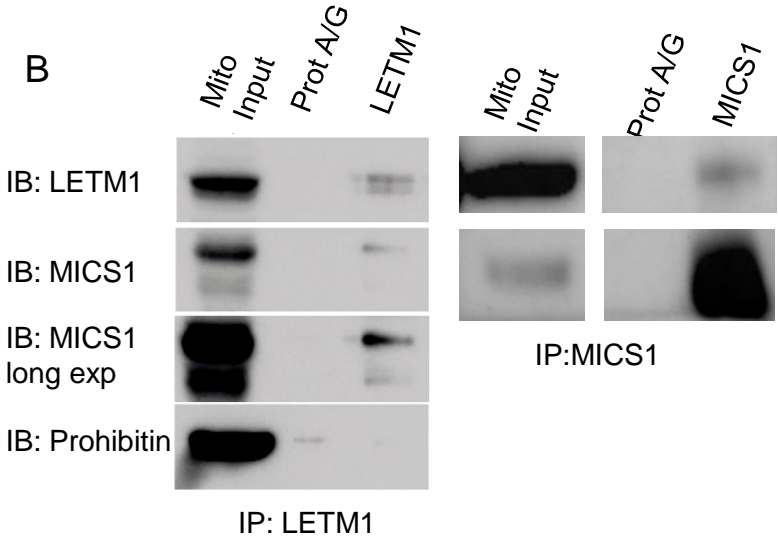
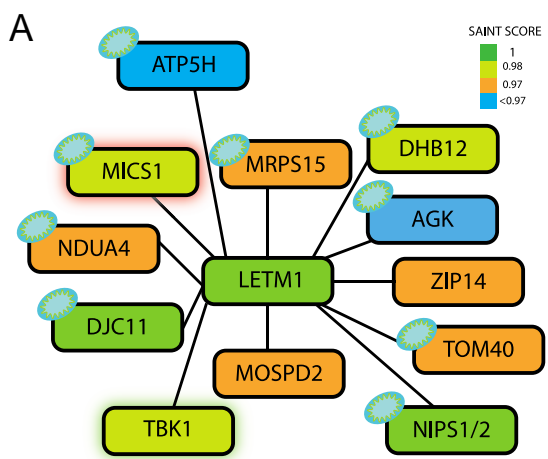
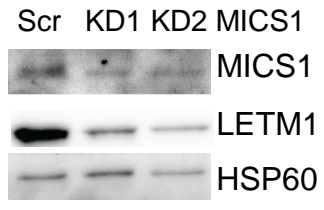
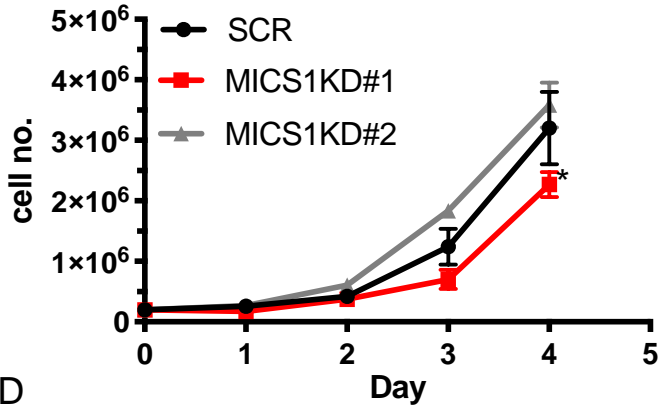


Figure 2

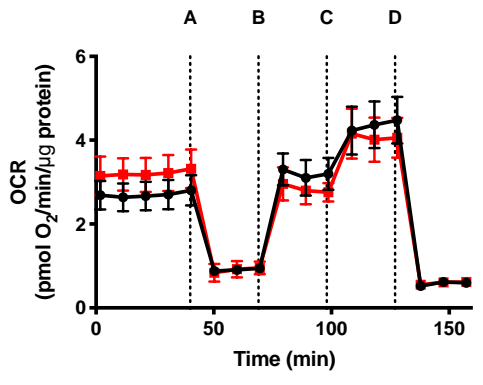
A



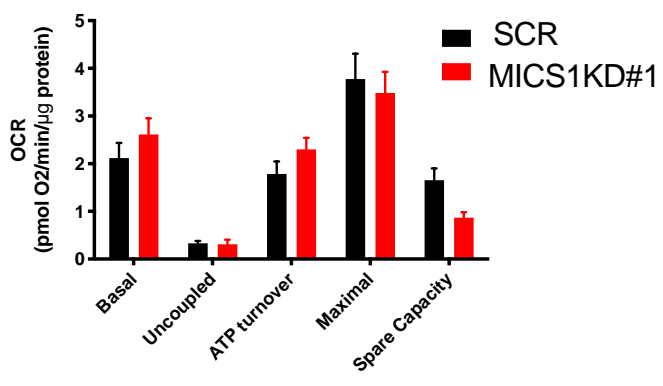
B



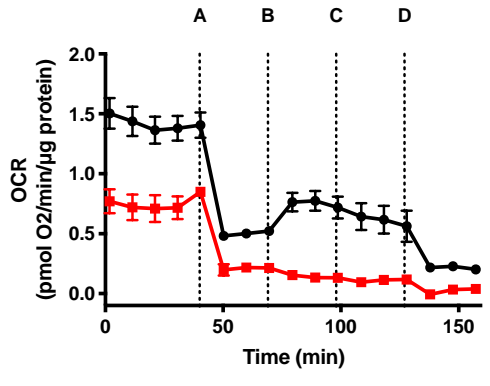
C



D



E



F

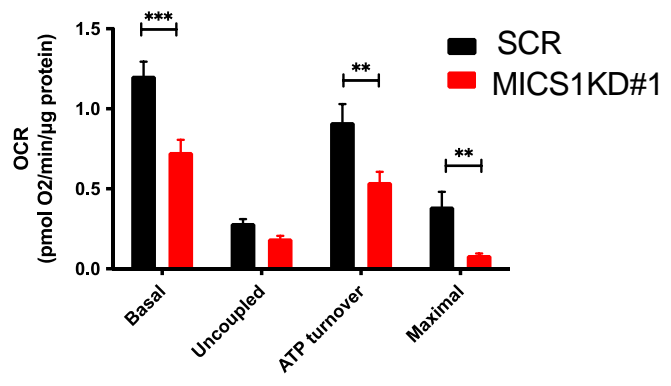




**Figure 3**

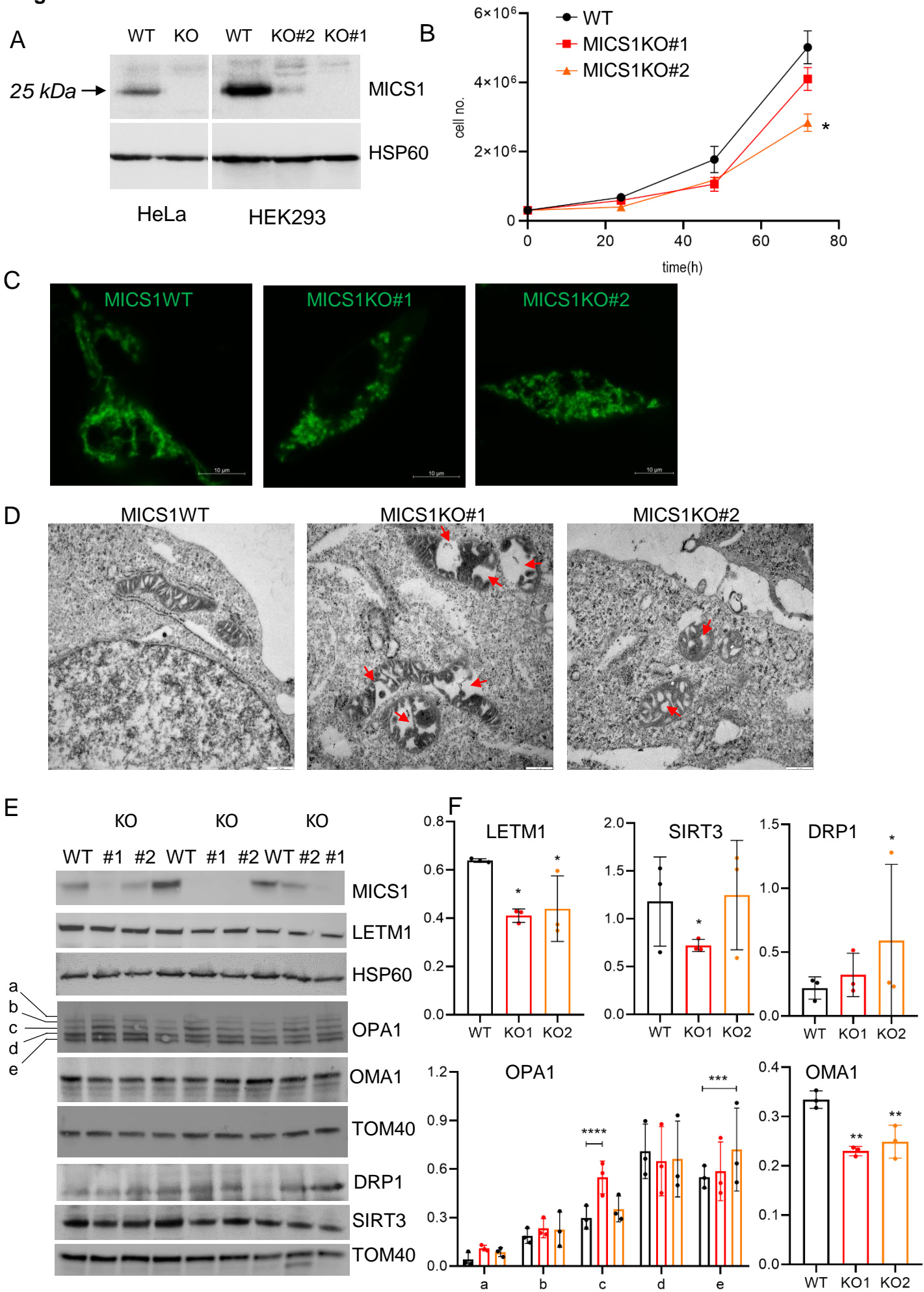


**Figure 4**

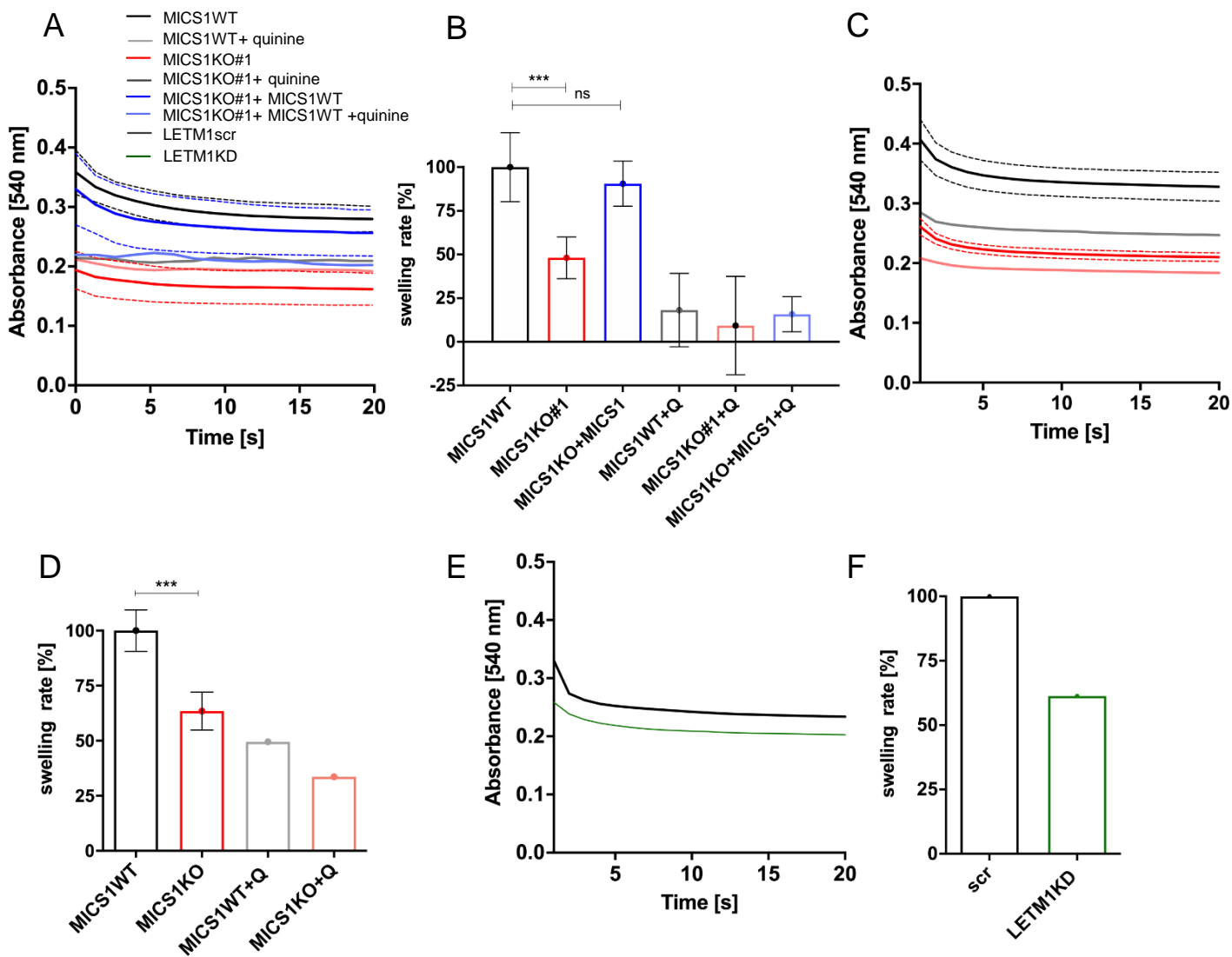
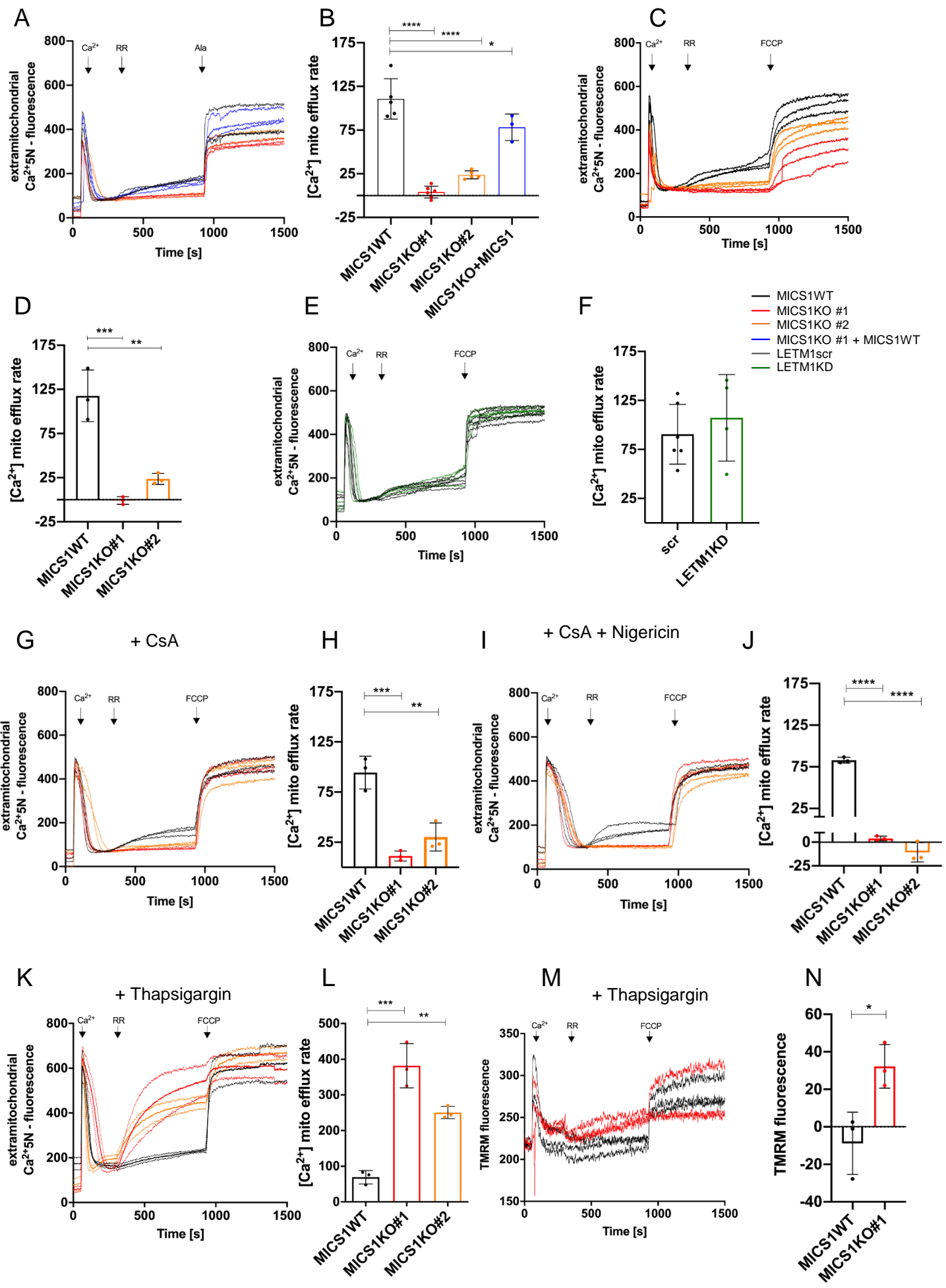
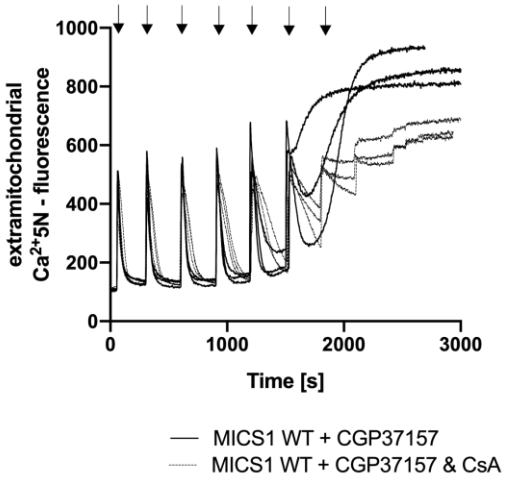


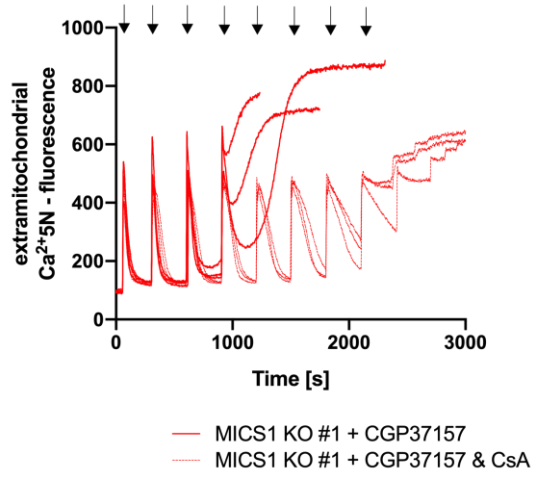
**Figure 5**



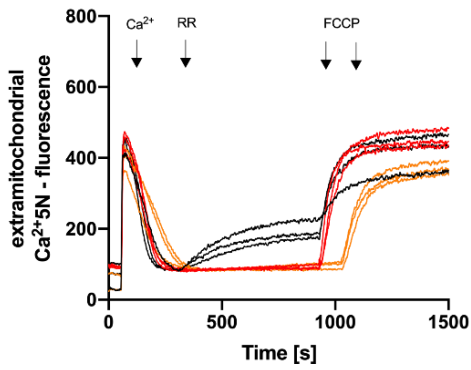
O + Thapsigargin



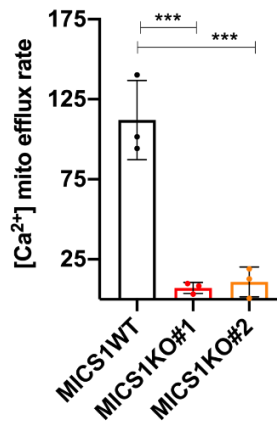
P + Thapsigargin



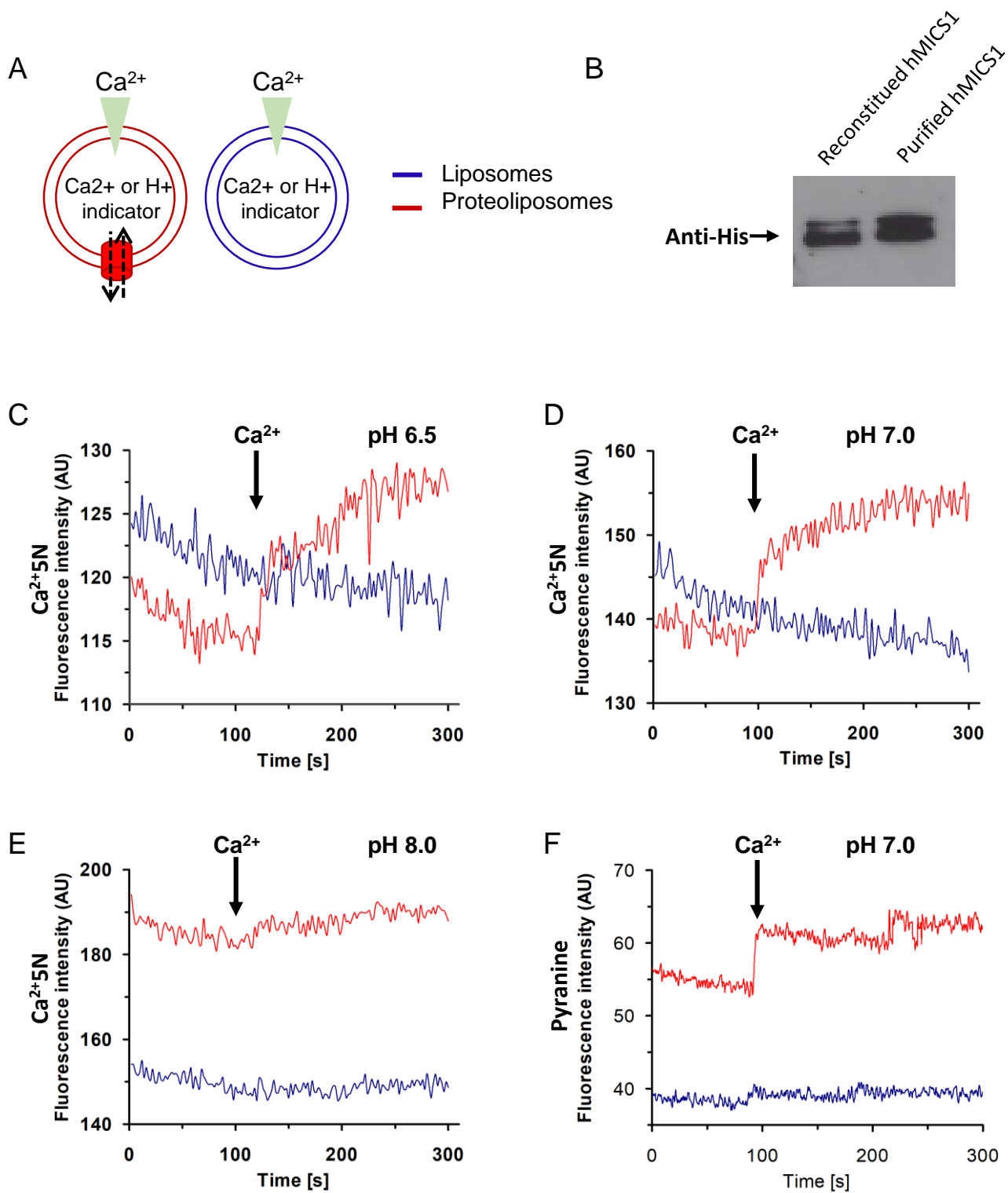
Q + Thapsigargin + CsA-ADP



R



**Figure 6**



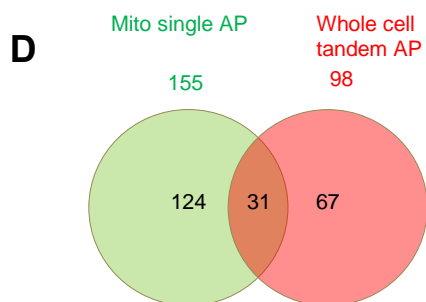
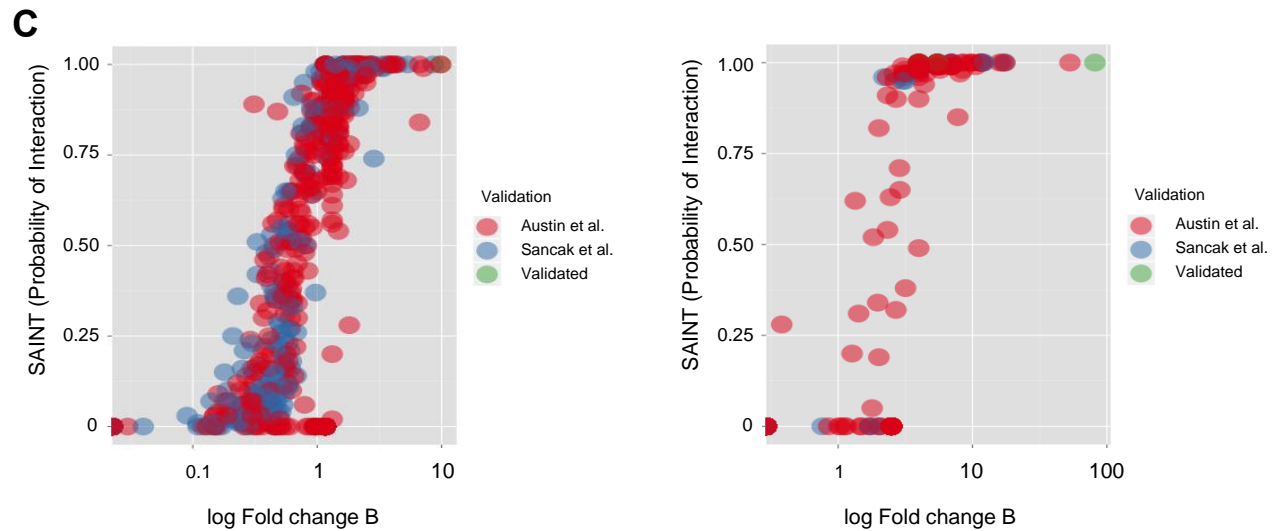
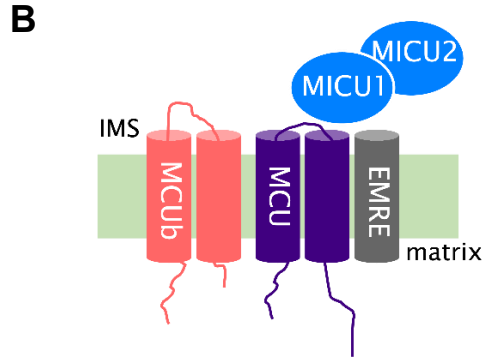
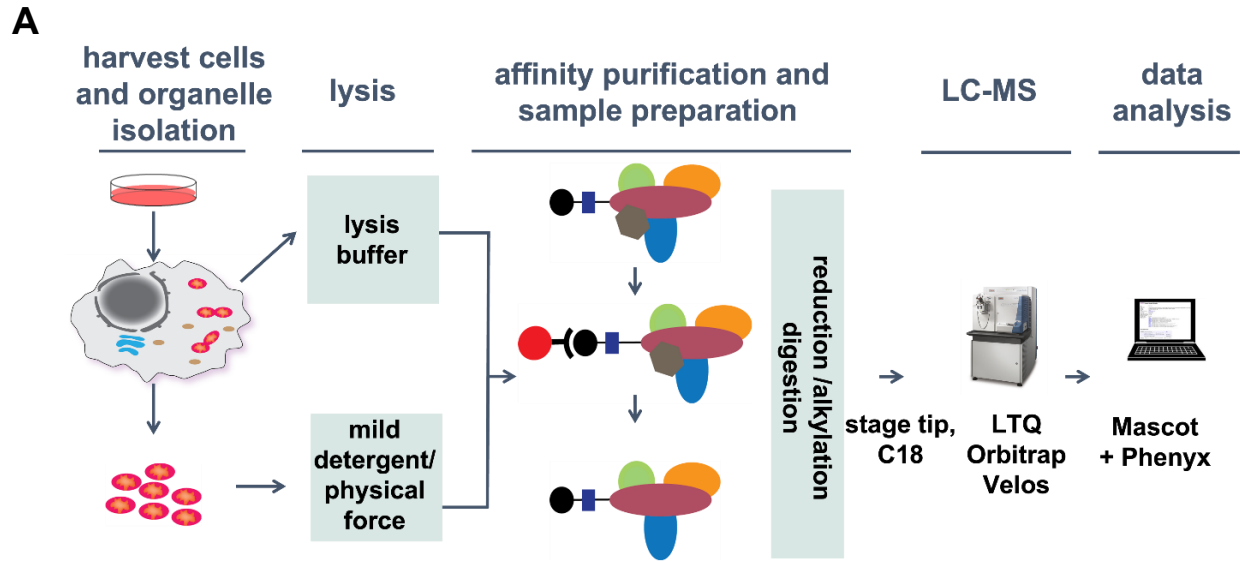
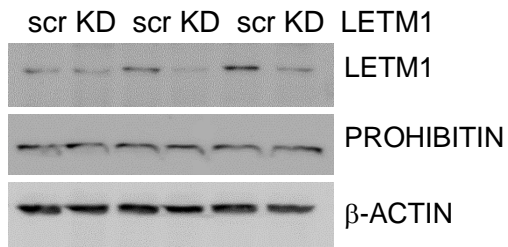


Figure 1-figure supplement 1

A



B

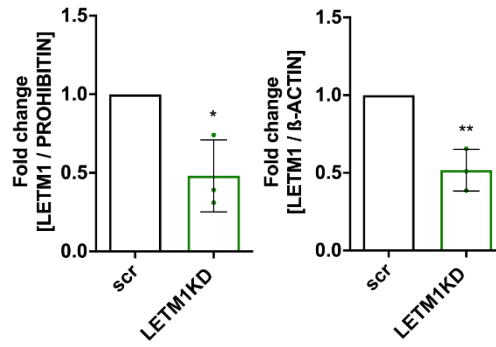


Figure 4- figure supplement 1

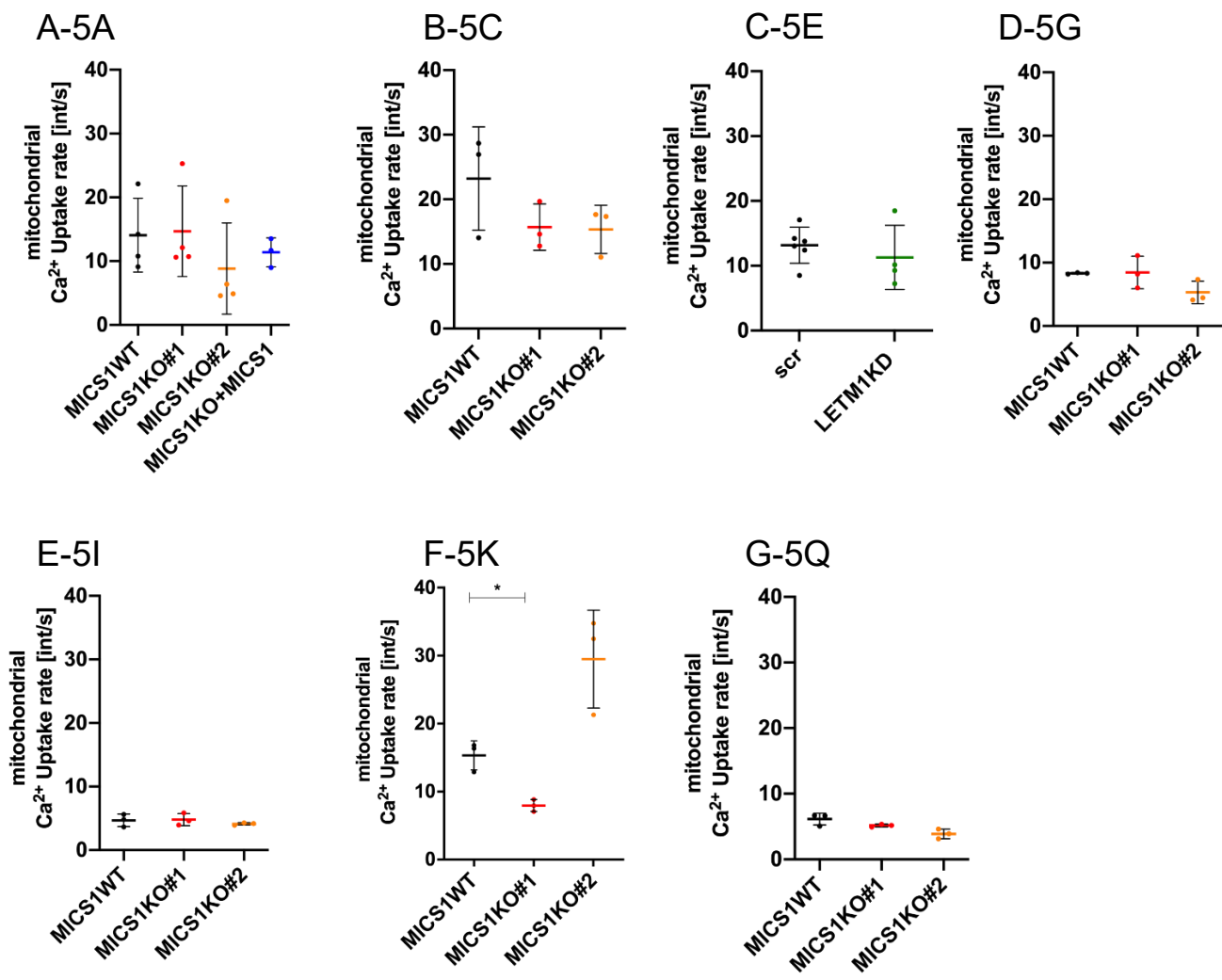


Figure 5-figure supplement 1



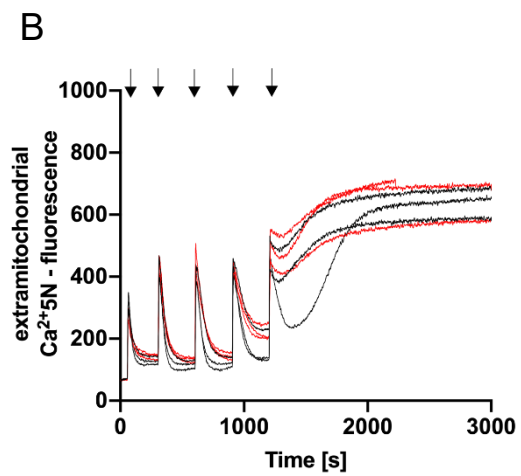
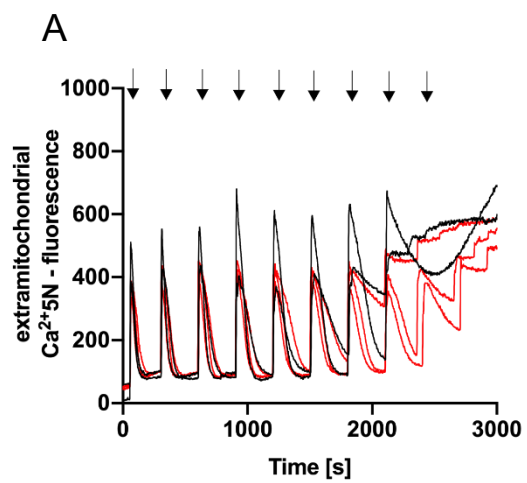


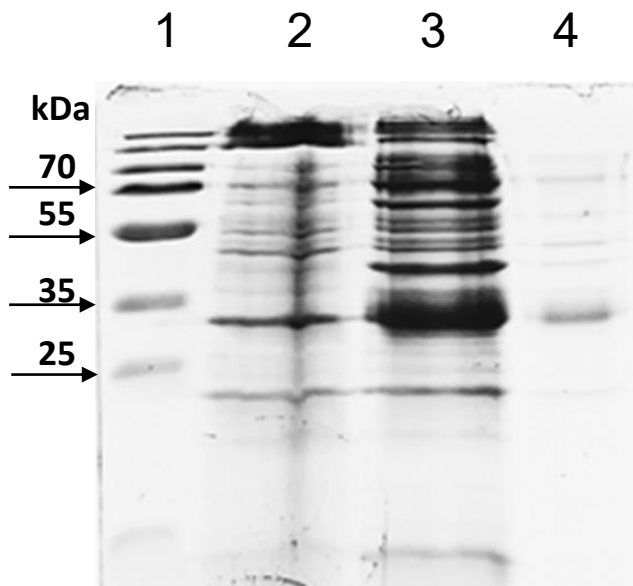
Figure 5-figure supplement 2

A

>Optimized\_MICS1

```
ATGCTGGCGGCGCGTCTGGTGTGCCTGCGTACCCTGCCGAGCCGTGTTTTCCATCCGGCG  
TTTACCAAAGCGAGCCCGGTTGTGAAGAACAGCATCACCAAGAACCAGTGGCTGCTGACC  
CCGAGCCGTGAGTACGCGACCAAACCCGTATCGGTATTCGTCGTGGCCGTACCGGTCAG  
GAGCTGAAGGAAGCGGCGCTGGAGCCGAGCATGGAAAAGATCTTCAAATGACCAAATG  
GGCCGTTGGTTCGTTGCGGGTGGCGCGGCGGTTGGTCTGGGTGCGCTGTGCTACTATGGT  
CTGGGCCTGAGCAACGAGATCGGTGCGATTGAAAAGGCGGTGATCTGGCCGCAGTATGTT  
AAAGATCGTATTCACAGCACCTACATGTATCTGGCGGGTAGCATTGGTCTGACCGCGCTG  
AGCGCGATCGCGATTAGCCGTACCCCGGTTCTGATGAACTTCATGATGCGTGGCAGCTGG  
GTGACCATCGGTGTTACCTTTGCGGCGATGGTGGGTGCGGGCATGCTGGTTCGTAGCATT  
CCGTATGACCAAAGCCCGGGTCCGAAACATCTGGCGTGGCTGCTGCACAGCGGCGTGATG  
GGTGCGGTGGTTGCGCCGCTGACCATTCTGGGTGGCCCGCTGCTGATTTCGTGCGGCGTGG  
TATACCGCGGGTATTGTGGGTGGCCTGAGCACCGTTGCGATGTGCGCGCCGAGCGAGAAA  
TTCCTGAACATGGGTGCGCCGCTGGGTGTTGGCCTGGGTCTGGTGTTCGTTAGCAGCCTG  
GGCAGCATGTTTCTGCCGCCGACCACCGTGGCGGGTGCAGCCCTGTACAGCGTTGCGATG  
TATGGTGGCCTGGTGTCTGTTTCTGCTGTACGATACCCAGAAAGTGATTTAA  
CGTGCGGAAGTTAGCCCGATGTACGGTGTGCAAAAATATGACCCGATCAACAGCATGCTG  
AGCATTTATATGGATACCCTGAACATTTTTTATGCGTGTGGCGACCATGCTGGCGACCGGC  
GGCAACCGTAAGAAA
```

B



C

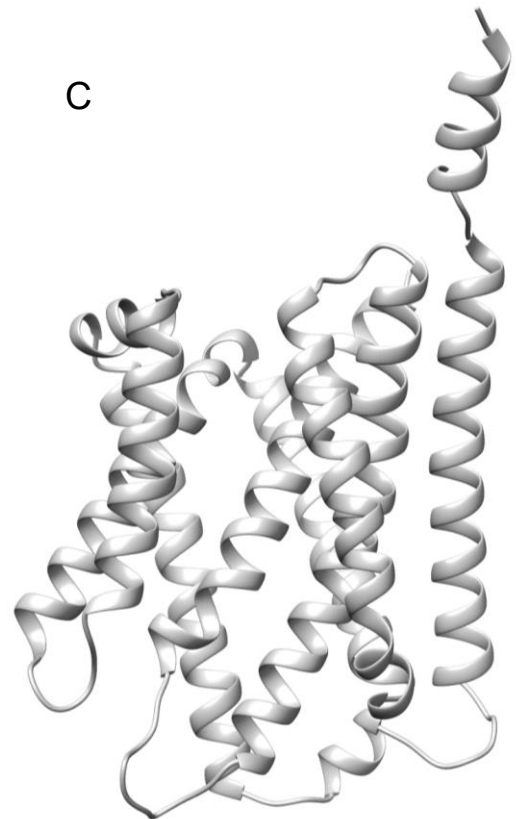


Figure 6-figure supplement 1

## Supplemental Figure titles and legends

### Figure 1- figure supplement 1

**AP-MS experiments** (A) Scheme illustrating workflow for minaturized AP-MS experiments, left to right: whole cells or isolated mitochondria are lysed or solubilized respectively. The cell/mitochondrial lysates are used for affinity purification (AP) using the StrepHA tag found on the bait protein. Eluates of the AP and control experiments are reduced, alkylated, and digested by trypsin. Peptides are purified on a C18 stage tip and then run on a LTQ Orbitrap Velos. Protein identifications were made by internal tools using MASCOT and Phenyx and removal of non-specific interactors done using the Crapome. (B) Mitochondrial calcium uniporter was selected as a model protein, the functional complex consist of the 5 proteins above (MCU, MCUb, MICU1, MICU2, EMRE). Note that an additional tissue-specific tertiary interaction partner (MICU3) (**2-4**), is only expressed at very low levels in HEK293 cells (Diego De Stefani, personal communication). Illustration adapted from Sancak et al. (C) Proteins identified by AP-MS were scored for probability of interaction using SAINT score and fold change B using raw data and the Crapome (left), proteins identified in Austin et al (red) and Sancak et al (blue). Both GFP & Crapome controls of similar experimental setup were used for analysis to filter nonspecific interactors (right), proteins identified in Austin et al (red), Sancak et al (blue) and validated interaction partners found in both (green). (D) Common affinity purification contaminants were eliminated from GFP and MCU analysis by removing proteins that had greater than 5 average spectral counts in the Crapome Database. (E) Venn diagram illustrating the number of proteins identified in mitochondrial single streptavidin AP (156 proteins) or whole cell tandem AP (98 proteins). While 31 proteins were found in common with both approaches, with 124 proteins being unique to the mitochondrial single streptavidin AP and 67 being unique to the whole cell tandem AP.

### Figure 4-figure supplement 1

**Downregulation of LETM1** (A) Western blot of HEK293 LETM1 scramble (scr) and LETM1KD (KD) used in Fig 4D-E. PROHIBITIN and  $\beta$ -ACTIN served as mitochondrial and total cellular loading control, respectively. (B) Statistics: unpaired two-sided t-test, \*p < 0.05, \*\*p < 0.01.

### Figure 5-figure supplement 1

**Mitochondrial Ca<sup>2+</sup> uptake rates.** The decay rate was calculated as exponential decrease of the Ca<sup>2+</sup> 5N Signals using the equation:  $Y = (Y_0 - \text{Plateau}) * \exp(-K * X) + \text{Plateau}$ , Rate of Decay/sec:  $K * Y_0$ ; X: Time (sec), Y: Starts at Y<sub>0</sub> (Ca<sup>2+</sup> peak) and decays with one phase down to Plateau; K: Rate constant equal to the reciprocal of the X axis units. Quantification of the Ca<sup>2+</sup> uptake rates recorded in Fig 5A (A), Fig 5C (B), Fig 5E (C), Fig 5G (D), Fig 5I (E), Fig 5K (F) and Fig 5P (G). Calculations were done using the GraphPad software and statistical analysis using Brown-Forsythe and Welch ANOVA, n=3, statistical analysis \*p < 0.05 for (F).

### Figure 5-figure supplement 2

**CRC in absence of CGP37157.** Permeabilized HEK293 MICS1 WT (black trace) and MICS1 KO (red trace) cells exposed (A) or not (B) to CsA were subjected to sequential Ca<sup>2+</sup> bolus of 5  $\mu$ M Ca<sup>2+</sup> while NCLX was not inhibited and fluorescence intensity was recorded.

## Figure 6-figure supplement 1

**MICS1 optimization, induction and structure overview.** A) Nucleotide sequence of the codon optimized sequence of MICS1 (B) MICS1 expression and purification. Lane 1: page ruler prestained plus marker; lane 2: insoluble fraction of not induced cell lysate (negative control); lane 3: insoluble fraction of cell lysate after 2 hours of 0.4 mM IPTG induction at 37 °C; lane 4: purified MICS1 protein. (C) Ribbon representation of the hMICS1 protein (Q9H3K2). PDB file retrieved from AlphaFold at <https://alphafold.ebi.ac.uk/entry/Q9H3K2>. The unstructured loop containing the first 55 amino acids has been removed.